Inorganic Chemistry

Article

pubs.acs.org/IC

Syntheses of Pentanuclear Group 6 Iridium Clusters by Core Expansion of Tetranuclear Clusters with $Ir(CO)_2(\eta^5\text{-}C_5Me_4R)$ (R = H, Me)†

Michael D. Randles,‡ Peter V. Simpson,‡ Vivek Gupta,‡ Junhong Fu,‡ Graeme J. Moxey,‡ Torsten Schwich,‡ Alan L. Criddle,‡ Simon Petrie,‡ Jonathan G. MacLellan,§ Stuart R. Batten,§ Robert Stranger,‡ Marie P. Cifuentes,‡ and Mark G. Humphrey*,‡

‡Research School of Chemistry, Australian National University (ANU), Canberra, ACT 0200, Australia

§School of Chemistry, Monash University, Clayton, Victoria 3800, Australia

Supporting Information

ABSTRACT: Metal cluster core expansion at tetrahedral group 6−group 9 mixed-metal clusters $MIr_3(\mu\text{-}CO)_3(CO)_8(\eta^5\text{-}L)$ (M = W, Mo, L = C_5H_5; M = Mo, L = C_5Me_5) with the iridium capping reagents $Ir(CO)_2(\eta^5\text{-}L')$ (L′ = C_5Me_5, C_5Me_4H) in refluxing toluene afforded the trigonal-bipyramidal clusters $MIr_4(\mu\text{-}CO)_3(CO)_7(\eta^5\text{-}C_5H_5)(\eta^5\text{-}L')$ (M = Mo, L′ = C_5Me_5, **1a**; M = W, L′ = C_5Me_5, **1b**; M = Mo, L′ = C_5Me_4H, **1c**; M = W, L′ = C_5Me_4H, **1d**) and $MoIr_4(\mu_3\text{-}H)(\mu\text{-}CO)_2(\mu\text{-}\eta^1\text{:}\eta^5\text{-}CH_2C_5Me_4)(CO)_7(\eta^5\text{-}C_5Me_5)$ (**2**). Related reactions with $M_2Ir_2(\mu\text{-}CO)_3(CO)_7(\eta^5\text{-}L)_2$ (M = W, Mo, L = C_5H_5; M = Mo, L = C_5Me_5) afforded $M_2Ir_3(\mu\text{-}CO)_3(CO)_6(\eta^5\text{-}C_5H_5)_2(\eta^5\text{-}L')$ (M = Mo, L′ = C_5Me_5, **3a**; M = W, L′ = C_5Me_5, **3b**; M = Mo, L′ = C_5Me_4H, **3c**; M = W, L′ = C_5Me_4H, **3d**), $W_2Ir_3(\mu\text{-}CO)_4(CO)_5(\eta^5\text{-}C_5H_5)_2(\eta^5\text{-}C_5Me_4H)$ (**4**), and $Mo_2Ir_3(\mu\text{-}CO)_3(CO)_6(\eta^5\text{-}C_5Me_5)_3$ (**5**). Single-crystal X-ray diffraction studies of **1a**−**1d**, **2**, **3a**−**3d**, and **4** confirmed their molecular structures, including the $\mu\text{-}\eta^1\text{:}\eta^5\text{-}CH_2C_5Me_4$ ligand at hydrido cluster **2**, derived from a C−H bond activation of one of the methyl groups. Density functional theory (DFT) studies were employed to suggest the structure of **5**. The redox behavior of the new clusters was examined through cyclic voltammetry; all clusters exhibit oxidation and reduction processes (with respect to the resting state), with the oxidation processes being the more reversible, and increasingly so on decreasing Ir content of the clusters, replacing W by Mo, and increasing alkylation of the cyclopentadienyl ligands. In situ IR and UV−vis−near-IR spectroelectrochemical studies of the reversible oxidation processes in **1a** and **3a** were undertaken, with the spectra of the former suggesting progression to an all-terminal CO geometry concomitant with the first oxidation and a significant structural change upon the second oxidation step. DFT studies of **1a** revealed that its crystallographically-confirmed Mo-equatorial core geometry is essentially isoenergetic with a possible Mo-apical isomer, and identified several bridging CO structures for the charged states.

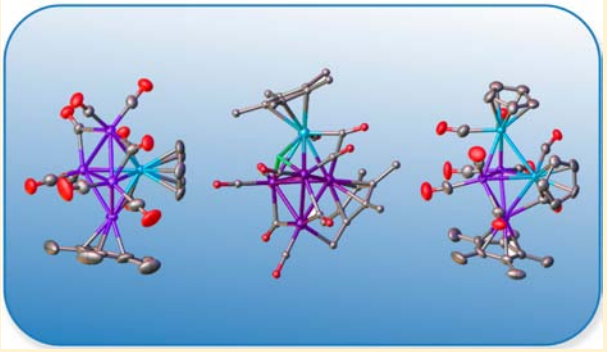

INTRODUCTION

Transition-metal carbonyl cluster complexes have been of long-standing interest.[1] The transition from molecular to bulk metal behavior that ensues with increasing cluster size is of fundamental interest, while the resultant possibility of achieving specific cluster-size-dependent properties may have practical use.[2] Clusters have long-recognized utility as models for catalytically active metal surfaces and as precursors for metal particles[3] and, more recently, have attracted interest for potential applications in optical limiting.[4]

Notwithstanding this fundamental and applied interest, and the resultant intensive study by many research groups over several decades, the metal carbonyl cluster field is still dominated by homometallic clusters and by heterometallic examples incorporating metals from the same group or from adjacent groups. Mixed-metal clusters incorporating disparate metals in the cluster core may possess certain advantageous properties: the polar M−M′ bonds may enhance organic substrate activation, and the clusters may be precursors for catalytically active heterometallic species with well-defined metal/metal stoichiometry and geometry.[5] Despite these attractive possibilities, the vast majority of such heterobimetallic clusters incorporating disparate metals contain three or four metal atoms; broadly applicable procedures to medium- and high-nuclearity examples are scarce, with notable exceptions being redox condensation,[6] bridge-assisted core expansion,[7] and particularly Stone's methodology employing alkylidene and alkylidyne ligands.[8] As archetypical examples, tri- and tetranuclear mixed-metal clusters containing metal atoms

Received: June 14, 2013
Published: September 23, 2013

   dx.doi.org/10.1021/ic401502f | *Inorg. Chem.* 2013, 52, 11256−11268

from groups 6 and 9 have attracted considerable interest,[9] but reports of higher-nuclearity examples incorporating metal atoms from these groups are sparse and frequently low-yielding and are restricted to specific targets;[10] this is despite significant desulfurization studies employing such clusters, as well as catalytic butane hydrogenolysis studies that revealed differing C−C selectivity for tungsten triiridium and ditungsten diiridium cluster precatalysts,[11] demonstrating the potential of mixed group 6−group 9 clusters in catalytically selective outcomes. Reliable procedures to higher-nuclearity examples are still required.

In studies directed at increasing the core nuclearity of clusters in this system, we previously reported high-yielding syntheses of trigonal-bipyramidal $M_2Ir_3(\mu_3\text{-}H)(\mu\text{-}CO)_2(CO)_9(\eta^5\text{-}C_5H_{5-m}Me_m)(\eta^5\text{-}C_5H_{5-n}Me_n)$ (M = Mo, W; m = 0, 4; n = 4, 5) and $M_2Ir_3(\mu_3\text{-}H)(\mu\text{-}CO)_2(CO)_9(\eta^5\text{-}C_5H_{5-n}Me_n)_2$ (M = Mo, W; n = 4, 5) from the redox-condensation reaction of the tetrahedral clusters $MIr_3(\mu\text{-}CO)_3(CO)_8(\eta^5\text{-}C_5H_{5-n}Me_n)$ (M = Mo, W; n = 0, 4) with the carbonylmetalate anions $[M(CO)_3(\eta^5\text{-}C_5H_{5-n}Me_n)]^-$ (M = Mo, W; n = 4, 5), followed by protonation.[12] We report herein studies exploring the utility of $Ir(CO)_2(\eta^5\text{-}C_5Me_4R)$ (R = H, Me) as a "capping" group in effecting a core-nuclearity increase in the Mo/W−Ir system, including single-crystal X-ray structural studies of most products, together with spectroscopic, electrochemical, spectroelectrochemical, and theoretical studies on the resultant fair- to high-yielding pentanuclear group 6−group 9 clusters.

EXPERIMENTAL DETAILS

General Conditions and Reagents. Reactions were performed under an atmosphere of nitrogen using standard Schlenk techniques. Product clusters proved indefinitely stable in air as solids and for at least short periods of time in solution, and thus no special precautions were taken to exclude air in their workup. Solvents used in reactions were AR-grade and distilled under nitrogen using standard methods: CH_2Cl_2 over CaH_2; toluene over sodium benzophenone ketyl. All other solvents were used as received. Petrol refers to a fraction of boiling range 60−80 °C. Cluster products were purified by preparative thin-layer chromatography (TLC) on 20 × 20 cm^2 glass plates coated with Merck GF_{254} silica gel (0.5 mm). Analytical TLC was conducted on aluminum sheets coated with 0.25 mm Merck GF_{254} silica gel. Literature procedures were used to synthesize $MoIr_3(\mu\text{-}CO)_3(CO)_8(\eta^5\text{-}C_5H_5)$,[9l] $MoIr_3(\mu\text{-}CO)_3(CO)_8(\eta^5\text{-}C_5Me_5)$,[9q] $WIr_3(CO)_{11}(\eta^5\text{-}C_5H_5)$,[11c] $Mo_2Ir_2(\mu_3\text{-}CO)(\mu\text{-}CO)_5(CO)_4(\eta^5\text{-}C_5H_5)_2$,[9n] $Mo_2Ir_2(\mu\text{-}CO)_3(CO)_7(\eta^5\text{-}C_5Me_5)_2$,[9q] $W_2Ir_2(CO)_{10}(\eta^5\text{-}C_5H_5)_2$,[11c] and $Ir(CO)_2(\eta^5\text{-}C_5Me_5)$.[13]

Instrumentation. IR spectra were recorded in AR-grade cyclohexane or CH_2Cl_2 on a Perkin-Elmer System 2000 FT-IR using a CaF_2 cell and are reported in reciprocal centimeters. ^1H NMR spectra were recorded on a Varian Gemini-300 spectrometer at 300 MHz in $CDCl_3$ (Cambridge Isotope Laboratories) and referenced to residual nondeuterated solvent (δ 7.26). Unit resolution and high-resolution electrospray ionization (ESI) mass spectrometry (MS) spectra were recorded on a Micromass-Waters LC-ZMD single-quadrupole liquid chromatography−mass spectrometer instrument. All MS values are reported in the form m/z (assignment, relative intensity). UV−vis spectra were recorded on a Cary 5 spectrophotometer. Microanalyses were carried out by the Microanalysis Service Unit in the Research School of Chemistry, ANU.

Synthesis of $[IrCl_2(\eta^5\text{-}C_5Me_4H)]_2$. 1,2,3,4-Tetramethylcyclopenta-1,3-diene (0.5 mL, 3.3 mmol) was added to a solution of $IrCl_3\cdot 3H_2O$ (1.0 g, 2.8 mmol) in methanol (50 mL), and the resultant solution was heated at reflux for 40 h. The mixture was allowed to return to room temperature before being cooled to 3 °C overnight. The resulting orange precipitate was isolated by filtration and washed with cold methanol (3 × 5 mL), yielding $[IrCl_2(\eta^5\text{-}C_5Me_4H)]_2$ (1.5 g, 1.9 mmol, 68%) as an orange powder, identified by comparison of the spectral data with literature values.[14]

Synthesis of $Ir(CO)_2(\eta^5\text{-}C_5Me_4H)$. $[IrCl_2(\eta^5\text{-}C_5Me_4H)]_2$ (0.50 g, 0.65 mmol) and CH_2Cl_2 (30 mL) were placed in a pressure bottle, and the mixture was flushed three times with 30 psi of CO and then pressurized to 40 psi of CO. The solution was stirred at room temperature for 3 h, the bottle was depressurized, and zinc dust (5 g) was added to the solution. The pressure bottle was once again flushed with CO (3 × 30 psi), pressurized to 40 psi, and stirred at room temperature for 16 h. The bottle was depressurized, and water (50 mL) was added to the solution. The mixture was stirred at room temperature for 1 h and then filtered to remove the zinc. The CH_2Cl_2 layer was separated and the aqueous layer washed with CH_2Cl_2 (3 × 20 mL). The combined CH_2Cl_2 extracts were dried over $MgSO_4$ and filtered, and the filtrate was taken to dryness in vacuo. The resultant brown residue was sublimed (85 °C, 0.1 mbar) to yield $Ir(CO)_2(\eta^5\text{-}C_5Me_4H)$ as a yellow-orange powder (0.10 g, 0.28 mmol, 43%), identified by comparison of the spectral data with literature values.[14]

Method A. *Synthesis of $MoIr_4(\mu\text{-}CO)_3(CO)_7(\eta^5\text{-}C_5H_5)(\eta^5\text{-}C_5Me_5)$ (**1a**).* $Ir(CO)_2(\eta^5\text{-}C_5Me_5)$ (127 mg, 331 μmol) was added to an orange solution of $MoIr_3(\mu\text{-}CO)_3(CO)_8(\eta^5\text{-}C_5H_5)$ (52 mg, 49.7 μmol) in toluene (15 mL), and the resultant mixture was heated at reflux for 1 h; the reaction was monitored by IR spectroscopy. The solution was taken to dryness in vacuo, and the crude residue was dissolved in the minimum amount of CH_2Cl_2 and applied to preparative silica TLC plates; elution with CH_2Cl_2/petrol (3:2) afforded four bands. The contents of the second (R_f = 0.46, brown) and fourth (R_f = 0.27, brown) bands were in trace amounts and were not isolated. The contents of the first band (R_f = 0.62, yellow) were extracted with CH_2Cl_2 and reduced in volume to afford a yellow solid identified as unreacted $Ir(CO)_2(\eta^5\text{-}C_5Me_5)$ (73.0 mg, 190 μmol, 57%). The contents of the third band (R_f = 0.34, red-brown) were extracted with CH_2Cl_2 and reduced in volume to afford a red-brown solid identified as **1a** (45.5 mg, 33.8 μmol, 68%). IR (CH_2Cl_2): ν(CO) 2053 s, 2024 s, 2008 vs, 1997 s sh, 1959 w, 1941 w, 1831 m br, 1797 m br, 1739 m br cm^{-1}. ^1H NMR: δ 5.05 (s, 5H, C_5H_5), 1.94 (s, 15H, C_5Me_5). MS (ESI): calcd, 1345 ($[M]^+$); found, 1345 ($[M]^+$, 100). Anal. Calcd for $C_{25}H_{20}Ir_4MoO_{10}$: C, 22.32; H, 1.50. Found: C, 22.21; H, 1.55.

*Synthesis of $WIr_4(\mu\text{-}CO)_3(CO)_7(\eta^5\text{-}C_5H_5)(\eta^5\text{-}C_5Me_5)$ (**1b**).* Following method A, $Ir(CO)_2(\eta^5\text{-}C_5Me_5)$ (10 mg, 26 μmol) and $WIr_3(CO)_{11}(\eta^5\text{-}C_5H_5)$ (16 mg, 14.1 μmol) in toluene (15 mL), refluxed for 25 min and preparative silica TLC elution with CH_2Cl_2/petrol (5:3), afforded six bands: the first band (R_f = 0.81, yellow) afforded orange unreacted $Ir(CO)_2(\eta^5\text{-}C_5Me_5)$ (2.3 mg, 5.9 μmol, 23%), the second band (R_f = 0.69, orange) afforded unreacted $WIr_3(CO)_{11}(\eta^5\text{-}C_5H_5)$ (5.2 mg, 4.6 μmol, 32%), and the third band (R_f = 0.41, red-brown) afforded red **1b** (5.6 mg, 3.9 μmol, 28%). IR (c-C_6H_{12}): ν(CO) 2055 s, 2030 s, 2010 vs, 1997 s, 1986 w, 1962 m, 1951 w, 1860 w, 1814 m, 1736 m cm^{-1}. ^1H NMR: δ 5.14 (s, 5H, C_5H_5), 1.93 (s, 15H, C_5Me_5). MS (ESI): calcd for $C_{25}H_{20}Ir_4O_{10}W$, 1436.9162 ($[M]^+$); found, 1436.9172 ($[M]^+$). Anal. Calcd for $C_{25}H_{20}Ir_4O_{10}W$: C, 20.95; H, 1.41. Found: C, 21.04; H, 1.49.

*Synthesis of $MoIr_4(\mu\text{-}CO)_3(CO)_7(\eta^5\text{-}C_5H_5)(\eta^5\text{-}C_5Me_4H)$ (**1c**).* Following method A, $Ir(CO)_2(\eta^5\text{-}C_5Me_4H)$ (8.0 mg, 21.6 μmol) and $MoIr_3(\mu\text{-}CO)_3(CO)_8(\eta^5\text{-}C_5H_5)$ (19.1 mg, 18.2 μmol) in toluene (15 mL), refluxed for 15 h and preparative silica TLC elution with dichloromethane/petrol (3:2), afforded two bands: the first band (R_f = 0.55, orange) afforded unreacted $MoIr_3(\mu\text{-}CO)_3(CO)_8(\eta^5\text{-}C_5H_5)$ (11.0 mg, 10.5 μmol, 57%), and the second band (R_f = 0.28, brown) afforded **1c** (6.7 mg, 5.02 μmol, 27%). IR (CH_2Cl_2): ν(CO) 2053 s, 2009 s, 1798 b, 1741 b, 1604 m cm^{-1}. MS (ESI): calcd for $C_{24}H_{18}Ir_4MoNaO_{10}$, 1358.8369 ($[M + Na]^+$); found, 1358.8370 ($[M + Na]^+$). ^1H NMR: δ 5.53 (s, 5H, C_5H_5), 5.10 (s, H, C_5HMe_4), 2.11 (s, 6H, C_5HMe_4), 1.89 (s, 6H, C_5HMe_4). Anal. Calcd for $MoC_{24}H_{18}Ir_4O_{10}$: C, 21.65; H, 1.36. Found: C, 21.80; H, 1.48.

*Synthesis of $WIr_4(\mu\text{-}CO)_3(CO)_7(\eta^5\text{-}C_5H_5)(\eta^5\text{-}C_5Me_4H)$ (**1d**).* Following method A, $Ir(CO)_2(\eta^5\text{-}C_5Me_4H)$ (13 mg, 35.1 μmol) and $WIr_3(CO)_{11}(\eta^5\text{-}C_5H_5)$ (11 mg, 9.7 μmol) in toluene (15 mL), refluxed for 30 min and preparative silica TLC elution with CH_2Cl_2/

dx.doi.org/10.1021/ic401502f | Inorg. Chem. 2013, 52, 11256−11268

petrol (5:3), afforded six bands: the third band (R_f = 0.41, red-brown) afforded red **1d** (3.9 mg, 2.7 μmol, 28%). IR (c-C_6H_{12}): ν(CO) 2055 m, 2031 m, 2012 s, 1996 m, 1986 w sh, 1963 w, 1957 w sh, 1866 w, 1819 w, 1736 s cm^{-1}. ^1H NMR: δ 5.38 (s, 1H, C_5Me_4H), 5.11 (s, 5H, C_5H_5), 1.88 (s, 6H, C_5Me_4H), 1.79 (s, 6H, C_5Me_4H). MS (ESI): calcd for $C_{24}H_{17}Ir_4O_{10}W$, 1443.8747 ($[M - H]^+$); found, 1443.8749 ($[M - H]^+$). Anal. Calcd for $C_{24}H_{18}Ir_4O_{10}W$: C, 20.31; H, 1.28. Found: C, 20.42; H, 1.35.

Synthesis of $MoIr_4(\mu_3\text{-}H)(\mu\text{-}CO)_2(\mu\text{-}\eta^1\text{:}\eta^5\text{-}CH_2C_5Me_4)(CO)_7(\eta^5\text{-}C_5Me_5)$ **(2)**. Following method A, $Ir(CO)_2(\eta^5\text{-}C_5Me_5)$ (33.4 mg, 87.1 μmol) and $MoIr_3(\mu\text{-}CO)_3(CO)_8(\eta^5\text{-}C_5Me_5)$ (12.2 mg, 10.9 μmol) in toluene (10 mL), refluxed for 1 h and preparative silica TLC elution with CH_2Cl_2/petrol (1:1) afforded two bands. The first band (R_f = 0.56, yellow) afforded unreacted $Ir(CO)_2(\eta^5\text{-}C_5Me_5)$ (18.2 mg, 47.5 μmol, 54%), and the second band (R_f = 0.43, red-brown) afforded **2** (10.4 mg, 7.35 μmol, 67%). IR (CH_2Cl_2): ν(CO) 2047 s, 2023 vs, 1988 vs br, 1914 w br, 1828 m br, 1787 s br cm^{-1}. ^1H NMR: δ 3.13 (s, 2H, CH_2), 2.01 (s, 15H, C_5Me_5), 1.51 (s, 6H, $C_5Me_4CH_2$), 1.08 (s, 6H, $C_5Me_4CH_2$), −4.21 (s, 1H, hydride). MS (ESI): calcd for $C_{29}H_{30}Ir_4MoO_9$, 1391.9462 ($[M]^+$); found, 1391.9463 ($[M]^+$). Anal. Calcd for $C_{29}H_{30}Ir_4MoO_9$: C, 25.11; H, 2.18. Found: C, 24.87; H, 2.00.

Synthesis of $Mo_2Ir_3(\mu\text{-}CO)_3(CO)_6(\eta^5\text{-}C_5H_5)_2(\eta^5\text{-}C_5Me_5)$ **(3a)**. Following method A, $Ir(CO)_2(\eta^5\text{-}C_5Me_5)$ (24.7 mg, 64.4 μmol) and $Mo_2Ir_2(\mu\text{-}CO)_3(CO)_7(\eta\text{-}C_5H_5)_2$ (42.9 mg, 43.5 μmol) in toluene (10 mL), refluxed for 30 min and preparative silica TLC elution with CH_2Cl_2/petrol (4:1) afforded two bands. The first band (R_f = 0.79, yellow) afforded unreacted $Ir(CO)_2(\eta^5\text{-}C_5Me_5)$ (2.1 mg, 5.5 μmol, 9%), and the second band (R_f = 0.27, purple-brown) afforded red-brown **3a** (46.5 mg, 36.2 μmol, 83%). IR (CH_2Cl_2): ν(CO) 2023 s, 1996 vs, 1966 m, 1949 w, 1903 w, 1890 w, 1835 m br, 1745 s br cm^{-1}. ^1H NMR: δ 5.21 (s, 5H, C_5H_5), 5.00 (s, 5H, C_5H_5), 1.95 (s, 15H, C_5Me_5). MS (ESI): calcd for $C_{29}H_{25}Ir_3Mo_2O_9$, 1286 ($[M]^+$); found, 1325 ($[M + K]^+$, 13), 1309 ($[M + Na]^+$, 100), 1286 ($[M]^+$, 78), 1258 ($[M - CO]^+$, 9). Anal. Calcd for $C_{29}H_{25}Ir_3Mo_2O_9$: C, 27.08; H, 1.96. Found: C, 26.90; H, 1.78.

Synthesis of $W_2Ir_3(\mu\text{-}CO)_3(CO)_6(\eta^5\text{-}C_5H_5)_2(\eta^5\text{-}C_5Me_5)$ **(3b)**. Following method A, $Ir(CO)_2(\eta^5\text{-}C_5Me_5)$ (17.4 mg, 45.3 μmol) and $W_2Ir_2(CO)_{10}(\eta^5\text{-}C_5H_5)_2$ (21.5 mg, 18.5 μmol) in toluene (15 mL), refluxed for 16 h and preparative silica TLC elution with CH_2Cl_2/petrol (4:1) afforded two bands. The first band (R_f = 0.74, yellow) afforded unreacted $Ir(CO)_2(\eta^5\text{-}C_5Me_5)$ (3.7 mg, 9.6 μmol, 21%), and the second band (R_f = 0.25, dark red) afforded **3b** (24.5 mg, 16.7 μmol, 90%). IR (CH_2Cl_2): ν(CO) 2054 vs, 2022 m, 1992 m, 1969 m, 1885 br, 1788 br cm^{-1}. ^1H NMR: δ 5.25 (s, 5H, C_5H_5), 5.05 (s, 5H, C_5H_5), 1.87 (s, 15H, C_5Me_5). MS (ESI): calcd for $C_{29}H_{26}Ir_3O_9W_2$, 1464.9484 ($[M + H]^+$); found, 1464.9484 ($[M + H]^+$, 12). Anal. Calcd for $C_{29}H_{25}Ir_3O_9W_2$: C, 23.83; H, 1.72. Found: C, 23.96; H, 1.76.

Synthesis of $Mo_2Ir_3(\mu\text{-}CO)_3(CO)_6(\eta^5\text{-}C_5H_5)_2(\eta^5\text{-}C_5Me_4H)$ **(3c)**. Following method A, $Ir(CO)_2(\eta^5\text{-}C_5Me_4H)$ (10.0 mg, 28.9 μmol) and $Mo_2Ir_2(\mu\text{-}CO)_3(CO)_7(\eta^5\text{-}C_5H_5)_2$ (19.0 mg, 19.3 μmol) in toluene (7 mL), refluxed for 1 h and preparative silica TLC elution with CH_2Cl_2/petrol (4:1) afforded two bands. The second band (R_f = 0.32, brown) afforded **3c** (16.6 mg, 13.0 μmol, 68%). IR (CH_2Cl_2): ν(CO) 2025 s, 1998 vs, 1969 m, 1951 w, 1895 w, 1821 m br, 1745 s br cm^{-1}. ^1H NMR: δ 5.39 (s, 1H, C_5Me_4H), 5.21 (s, 5H, C_5H_5), 5.02 (s, 5H, C_5H_5), 2.05 (s, 6H, C_5Me_4H), 1.92 (s, 6H, C_5Me_4H). MS (ESI): calcd for $C_{28}H_{23}Ir_3Mo_2O_9$, 1277.8338 ($[M]^+$); found, 1277.8335 ($[M]^+$). Anal. Calcd for $C_{28}H_{23}Ir_3Mo_2O_9$: C, 26.44; H, 1.82. Found: C, 26.62; H, 1.95.

Synthesis of $W_2Ir_3(\mu\text{-}CO)_3(CO)_6(\eta^5\text{-}C_5H_5)_2(\eta^5\text{-}C_5Me_4H)$ **(3d)** *and* $W_2Ir_3(\mu\text{-}CO)_4(CO)_5(\eta^5\text{-}C_5H_5)_2(\eta^5\text{-}C_5Me_4H)$ **(4)**. Following method A, $Ir(CO)_2(\eta^5\text{-}C_5Me_4H)$ (19.2 mg, 52.0 μmol) and $W_2Ir_2(CO)_{10}(\eta^5\text{-}C_5H_5)_2$ (37.0 mg, 31.8 μmol) in toluene (20 mL), refluxed for 15 h and preparative silica TLC elution with CH_2Cl_2/petrol (4:1) afforded two bands. The first band (R_f = 0.75, yellow) afforded unreacted $Ir(CO)_2(\eta^5\text{-}C_5Me_4H)$ (3.2 mg, 8.67 μmol, 16.7%), and the second band (R_f = 0.38, dark red) afforded **4** (16.8 mg, 11.6 μmol, 37%). IR (CH_2Cl_2): ν (CO) 2054 s, 2025 s, 2001 s, 1968 s, 1886 b, 1808 b, 1732 s cm^{-1}. MS (ESI): calcd for $C_{28}H_{23}Ir_3NaO_9W_2$, 1472.9147 ($[M + Na]^+$); found, 1472.9148 ($[M + Na]^+$). ^1H NMR: δ 5.42 (s, 5H, C_5H_5), 5.12 (s, 5H, C_5H_5), 4.98 (s, H, C_5HMe_4), 2.13 (s, 6H, C_5HMe_4), 1.73 (s, 6H, C_5HMe_4). Anal. Calcd for $C_{28}H_{23}Ir_3O_9W_2$: C, 23.23; H, 1.60. Found: C, 23.58; H, 1.72. The third band (R_f = 0.35, dark red) afforded **3d** (4.5 mg, 3.10 μmol, 10%). IR (CH_2Cl_2): ν(CO) 2054 s, 2021 m, 1994 s, 1969 b, 1885 b, 1789 b cm^{-1}. MS (ESI): calcd for $C_{28}H_{23}Ir_3O_9W_2$, 1449; found, 1449 ($[M]^+$, 35), 1472 ($[M + Na]^+$, 75), 1421 ($[M - CO]^+$, 5). ^1H NMR ($CDCl_3$): δ 5.42 (s, 5H, C_5H_5), 5.26 (s, 5H, C_5H_5), 5.09 (s, H, C_5HMe_4), 2.20 (s, 6H, C_5HMe_4), 1.94 (s, 6H, C_5HMe_4). Anal. Calcd for $C_{28}H_{23}Ir_3O_9W_2$: C, 23.23; H, 1.60. Found: C, 23.41; H, 1.68.

Synthesis of $Mo_2Ir_3(\mu\text{-}CO)_3(CO)_6(\eta^5\text{-}C_5Me_5)_3$ **(5)**. Following method A, $Ir(CO)_2(\eta^5\text{-}C_5Me_5)$ (12.7 mg, 33.1 μmol) and $Mo_2Ir_2(\mu\text{-}CO)_3(CO)_7(\eta^5\text{-}C_5Me_5)_2$ (5.7 mg, 5.1 μmol) in toluene (5 mL), refluxed for 1 h and preparative silica TLC elution with CH_2Cl_2/petrol (3:2) afforded two bands. The first band (R_f = 0.64, yellow) afforded unreacted $Ir(CO)_2(\eta^5\text{-}C_5Me_5)$ (4.3 mg, 11.2 μmol, 34%), and the second band (R_f = 0.50, brown-green) afforded **5** (4.1 mg, 2.87 μmol, 57%). IR (CH_2Cl_2): ν(CO) 2011 s, 1983 vs, 1960 m, 1938 w, 1827 w br, 1681 m br cm^{-1}. ^1H NMR: δ 1.97 (s, 30H, C_5Me_5), 1.86 (s, 15H, C_5Me_5). MS (ESI): calcd for $C_{39}H_{45}Ir_3Mo_2O_9$, 1432.0060 ($[M]^+$); found, 1432.0090 ($[M]^+$). Anal. Calcd for $C_{39}H_{45}Ir_3Mo_2O_9$: C, 32.84; H, 3.18.Found: C, 33.13; H, 3.00.

Cyclic Voltammetry. Cyclic voltammetry measurements were recorded using an EA161 potentiostat and e-corder from eDaq Pty Ltd. Measurements were carried out at room temperature using platinum disk working, platinum wire auxiliary, and Ag/AgCl reference electrodes, such that the ferrocene/ferrocenium redox couple was located at 0.56 V (i_{pc}/i_{pa} = 1; ΔE_p 0.09 V). Scan rates were typically 100 mV s^{-1}. Electrochemical solutions contained 0.1 M $(NBu^n_4)PF_6$ and ca. 10^{-3} M complex in dried and distilled dichloromethane. Solutions were purged and maintained under a nitrogen atmosphere.

Spectroelectrochemical Studies. Electronic spectra were recorded using a Cary 5 spectrophotometer, and IR spectra were recorded on a Perkin-Elmer System 2000 spectrometer. Solution spectra of the oxidized species were obtained at 298 K by electrogeneration in optically transparent thin-layer electrochemical (OTTLE) cells with potentials of ca. 50−200 mV beyond $E_{1/2}$ for each couple, to ensure complete electrolysis. Solutions were made up using 0.3 M $(NBu^n_4)PF_6$ in dried and distilled dichloromethane.

X-ray Crystallographic Studies. *General Procedures.* The crystal and refinement data for compounds **1a**−**1d**, **2**, **3a**−**3d**, and **4** are summarized in Table S1 in the Supporting Information (SI). Crystals suitable for the X-ray structural analyses were grown by liquid diffusion of methanol into a dichloromethane solution (**1b**−**1d**, **3b**, **3d**, and **4**), liquid diffusion of ethanol into a dichloromethane solution (**1a**), or liquid diffusion of ethanol into a chloroform solution (**2**, **3a**, and **3c**) at 277 K. Suitable crystals were mounted on fine glass capillaries, and intensity data were collected on a Nonius KAPPA CCD diffractometer at 200 K (all except **3c**), or a Bruker Apex II CCD diffractometer at 123 K (**3c**), using graphite-monochromated Mo Kα radiation (λ = 0.71073 Å). N_t (total) reflections were measured by using ψ and ω scans and were reduced to N_o unique reflections, with $F_o > 2\sigma(F_o)$ being considered to be observed. Data were initially processed and corrected for absorption by using the programs *DENZO*[15] and *SORTAV*[16] (all except **3c**) or the *Apex II* program suite[17] (**3c**). The structures were solved by using direct methods and observed reflections were used in least-squares refinement on F^2, with anisotropic thermal parameters refined for non-hydrogen atoms. With the exception of the bridging hydride (H41) in **2**, which was located in the difference Fourier map, hydrogen atoms were constrained in calculated positions and refined with a riding model. Structure solutions and refinements were performed by using the *CRYSTALS* software package[18] (**1a**, **1b**, **1d**, **2**, and **3a**) or the programs *SHELXS-97* and *SHELXL-97*[19] through the graphical interface *Olex2*[20] (**1c**, **3b**, **3c**, **3d**, **4**), which was also used to generate the figures. In all structures, the largest peaks in the final difference electron map are located near the metal atoms.

Variata. **1a**. The crystallographic asymmetric unit consists of the cluster and half of a dichloromethane solvent molecule, with the other

Scheme 1. Syntheses of 1−5

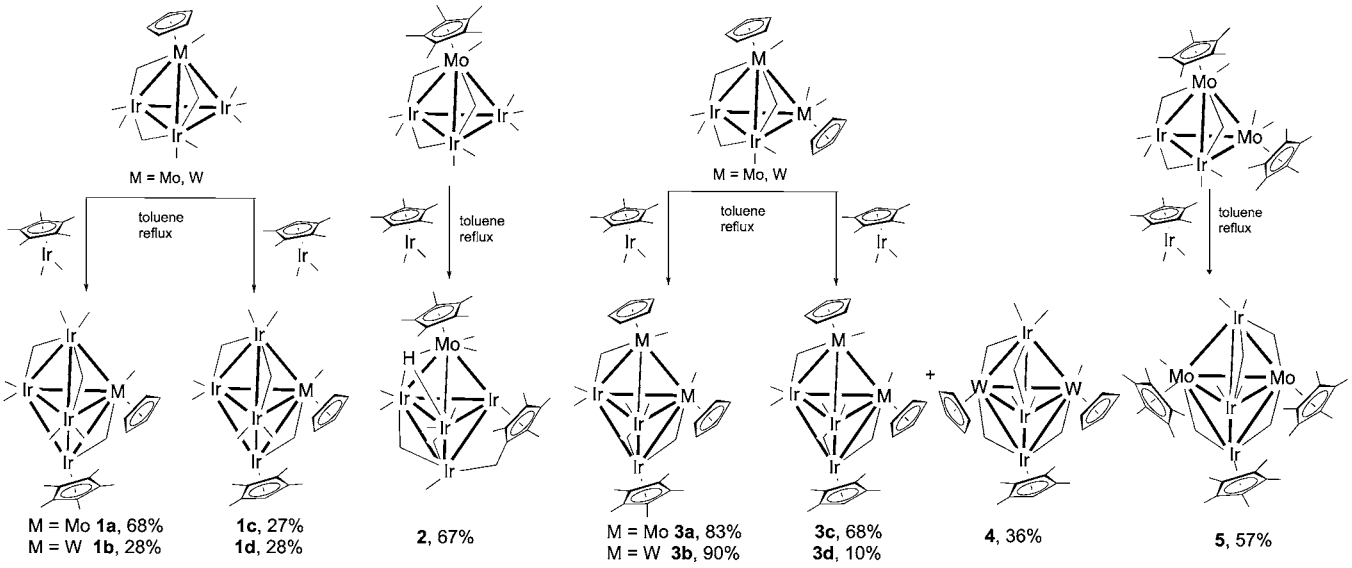

half being generated by 2-fold rotation axes that pass through the carbon and chlorine atoms. Bond length and angle restraints were applied to the lattice dichloromethane molecule.

1b. The unit cell of **1b** contains four dichloromethane molecules that have been treated as a diffuse contribution to the overall scattering without specific atom positions by *PLATON SQUEEZE*.[21] Restraints were applied to the cyclopentadienyl and pentamethylcyclopentadienyl rings to ensure planarity of the rings and ring C−C bond distances of ca. 1.41 Å. Two of the methyl groups displayed large thermal ellipsoids, so restraints were employed.

2. The crystal diffracted weakly and no reflection data were observed at high angles, so the maximum θ value was reduced to 22.5° in the refinement.

3d. The anisotropic displacement parameters of cyclopentadienyl and tetramethylcyclopentadienyl ligands were restrained. *PLATON SQUEEZE*[21] was used to check for the presence of dichloromethane in the crystal voids. Insufficient electron density was located in the voids to indicate the presence of dichloromethane, so this electron density was not removed from the refinement.

Theoretical Studies. Computational studies were carried out using the *Amsterdam Density Functional* (ADF) program, version 2010.02,[22] typically running on four or eight cores on local, Linux-based workstations. The calculations employed all-electron basis sets of triple-ζ quality with a single polarization function (TZP) on each atom. All calculations employed the local density approximation (LDA)[23] to the exchange and correlation potentials of Vosko, Wilk, and Nusair[24] for geometry optimizations. As we have previously shown,[9q,s,u,11,25] the LDA methodology provides superior geometry optimization of these types of systems where significant metal−metal bonding is involved. The hybrid B3LYP functional[26] was employed for the calculation of single-point energies based on the LDA-optimized structures. Relativistic effects were accounted for using the zero-order relativistic approximation (ZORA).[27] The fluxionality of carbonyl ligands in these systems necessitated the use of nonstandard (tighter) convergence parameters, consisting of 2×10^{-4} hartree for energy, 10^{-2} hartree/Å for gradients, and a numerical integration accuracy exponent of 4.0. Some ZORA-corrected PBE/TZP optimizations were repeated with the inclusion of solvent effects through the conductor-like screening model (COSMO) method, using parameters appropriate to solvation by dichloromethane.

RESULTS AND DISCUSSION

Syntheses and Spectroscopic Characterization. The reaction of $Ir(CO)_2(\eta^5\text{-}C_5Me_5)$ with $MoIr_3(\mu\text{-}CO)_3(CO)_8(\eta^5\text{-}C_5H_5)$ in refluxing toluene for 1 h, followed by preparative TLC, afforded one major product in 68% yield, identified by an X-ray structural study as the trigonal-bipyramidal cluster **1a**. An analogous reaction using $WIr_3(CO)_{11}(\eta^5\text{-}C_5H_5)$ afforded **1b**, albeit in much lower yield. The related capping agent $Ir(CO)_2(\eta^5\text{-}C_5Me_4H)$ was prepared in two steps from commercial $IrCl_3\cdot 3H_2O$: Reaction with 1,2,3,4-tetramethylcyclopenta-1,3-diene afforded $[IrCl_2(\eta^5\text{-}C_5Me_4H)]_2$, the carbonylation of which (in the presence of zinc as reducing agent) gave $Ir(CO)_2(\eta^5\text{-}C_5Me_4H)$. The reaction of $MoIr_3(\mu\text{-}CO)_3(CO)_8(\eta^5\text{-}C_5H_5)$ or $WIr_3(CO)_{11}(\eta^5\text{-}C_5H_5)$ with excess $Ir(CO)_2(\eta^5\text{-}C_5Me_4H)$ proceeded in a manner analogous to that of the $Ir(CO)_2(\eta^5\text{-}C_5Me_5)$ examples, giving $MIr_4(\mu\text{-}CO)_3(CO)_7(\eta^5\text{-}C_5H_5)(\eta^5\text{-}C_5Me_4H)$ (M = Mo, **1c**; M = W, **1d**; Scheme 1). The new clusters were characterized by IR and ^{1}H NMR spectroscopy, ESI MS, satisfactory microanalyses, and single-crystal X-ray diffraction studies. The solution IR spectra in CH_2Cl_2 contain 9 or 10 ν(CO) bands, 6 or 7 of which correspond to terminally bound carbonyls (2055−1941 cm^{-1}) and 3 to bridging carbonyl modes (1866−1736 cm^{-1}). The ^{1}H NMR spectra contain resonances assigned to the various cyclopentadienyl groups, while intense molecular-ion peaks with the correct characteristic isotope patterns are seen in the ESI MS spectra.

The reaction of the sterically more demanding tetranuclear precursor $MoIr_3(\mu\text{-}CO)_3(CO)_8(\eta^5\text{-}C_5Me_5)$ with excess $Ir(CO)_2(\eta^5\text{-}C_5Me_5)$ was also examined. Interestingly, the major product from this reaction, **2** (67%), contains the iridium reagent residue in an equatorial rather than an axial position at the trigonal-bipyramidal core, with one of its pentamethylcyclopentadienyl methyl groups having undergone C−H bond activation to afford σ-methylene and face-capping hydride units. Complex **2** was characterized by IR and ^{1}H NMR spectroscopy, ESI MS, satisfactory microanalysis, and a single-crystal X-ray diffraction study. The solution IR spectrum in CH_2Cl_2 contains six ν(CO) bands, four of which correspond to terminal (2047−1914 cm^{-1}) and two to bridging carbonyl ligands (1828 and 1787 cm^{-1}). The ^{1}H NMR spectrum contains one resonance assigned to the molybdenum-bound pentamethylcyclopentadienyl group at δ 2.01, three resonances at δ 3.13, 1.51, and 1.08 in a ratio of 2:6:6 attributed to the iridium-ligated (tetramethylcyclopentadienyl)methyl, and a hydride ligand

dx.doi.org/10.1021/ic401502f | *Inorg. Chem.* 2013, 52, 11256−11268

resonance at δ −4.21. A molecular-ion peak with the correct characteristic isotope pattern is seen at 1387 mass units in the ESI MS spectrum.

The clusters $Mo_2Ir_2(\mu\text{-}CO)_3(CO)_7(\eta^5\text{-}C_5H_5)_2$ and $W_2Ir_2(CO)_{10}(\eta^5\text{-}C_5H_5)_2$, related to $MoIr_3(\mu\text{-}CO)_3(CO)_8(\eta^5\text{-}C_5H_5)$ and $WIr_3(CO)_{11}(\eta^5\text{-}C_5H_5)$ by isolobal replacement of $Ir(CO)_3$ by $M(CO)_2(\eta^5\text{-}C_5H_5)$, were reacted with $Ir(CO)_2(\eta^5\text{-}C_5Me_5)$ in refluxing toluene over 1 h to afford the trigonal-bipyramidal clusters $M_2Ir_3(\mu\text{-}CO)_3(CO)_6(\eta^5\text{-}C_5H_5)_2(\eta^5\text{-}C_5Me_5)$ (M = Mo, **3a**; M = W, **3b**). Analogous reactions employing $Ir(CO)_2(\eta^5\text{-}C_5Me_4H)$ yielded $M_2Ir_3(\mu\text{-}CO)_3(CO)_6(\eta^5\text{-}C_5H_5)_2(\eta^5\text{-}C_5Me_4H)$ (M = Mo, **3c**; M = W, **3d**). Interestingly, from the reaction between $Ir(CO)_2(\eta^5\text{-}C_5Me_4H)$ and $W_2Ir_2(\mu\text{-}CO)_3(CO)_7(\eta^5\text{-}C_5H_5)_2$, the cluster **4** was isolated in addition to **3d**; cluster **4** features two tungsten atoms in equatorial positions of the trigonal-bipyramidal cluster core and four bridging carbonyl ligands. The treatment of $Mo_2Ir_2(\mu\text{-}CO)_3(CO)_7(\eta^5\text{-}C_5Me_5)_2$ with $Ir(CO)_2(\eta^5\text{-}C_5Me_5)$ in refluxing toluene afforded **5**. Complexes **3a**−**3d**, **4**, and **5** were characterized by IR and ^{1}H NMR spectroscopy, ESI MS, and satisfactory microanalyses. Single-crystal X-ray diffraction studies conclusively established the structures for **3a**−**3d** and **4**; the geometry of **5** was suggested by density functional theory (DFT) calculations (see below). The solution IR spectra of **3a**−**3d** in CH_2Cl_2 contain six to eight ν(CO) bands, five or six of which correspond to terminally bound carbonyls (2025−1890 cm^{-1}) and one or two to bridging carbonyl modes (1835−1745 cm^{-1}), while that of **4** contains five ν(CO) bands corresponding to terminal CO ligand stretching modes and two ν(CO) bands corresponding to bridging carbonyls. The ^{1}H NMR spectra contain resonances assigned to the various cyclopentadienyl groups, while intense molecular-ion peaks and adduct-ion peaks corresponding to the addition of sodium or potassium ions are detected in the ESI MS spectra.

X-ray Structural Studies of 1a−1d, 2, 3a−3d, and 4. Single-crystal X-ray diffraction studies confirmed the molecular compositions of **1a**−**1d**, **2**, **3a**−**3d**, and **4**. ORTEP plots with the molecular structure and atomic labeling schemes for **1d**, **2**, **3c**, and **4** are shown in Figures 1−4, respectively. Figures S1 (**1a**), S2 (**1b**), S3 (**1c**), S4 (**3a**), S5 (**3b**), and S6 (**3d**) in the SI contain ORTEP plots from the remaining structural studies. Table S1 in the SI contains crystallographic data acquisition and refinement parameters, Table 1 lists selected bond distances for **1a**−**1d**, and Table 2 lists selected bond distances for **3a**−**3d**, with selected bond distances for **2** and **4** being given in the respective figure captions.

The metal cores of **1**−**4** adopt trigonal-bipyramidal geometries with the group 6 metals ligated by η^5-cyclopentadienyl/η^5-pentamethylcyclopentadienyl groups and the incoming $Ir(\eta^5\text{-}C_5Me_nH_{5-n})$ (n = 4, 5) unit either in an apical site, capping one of the MIr_2 (M = Mo, W: **1a**−**1d**, **3a**−**3d**) or W_2Ir (**4**) faces, or in an equatorial site (**2**). The clusters contain three or four bridging and six or seven terminally bound carbonyl ligands. All possess 72 cluster valence electrons, and so are EAN-precise for M_5 clusters possessing nine M−M bonds. Note that there is local electronic asymmetry; assigning the electrons from each ligand to the metal atom to which they are bound, a symmetrical distribution of the electrons from the bridging CO ligands, and assigning face-capping hydride H41 to Mo4 in **2**, there is residual electronic asymmetry in **2** (Ir1, 19 e; Ir5, 17 e), **3** (Ir4, 19 e; Mo5, 17 e), and **4** (W2, 17 e; Ir4, 19 e).

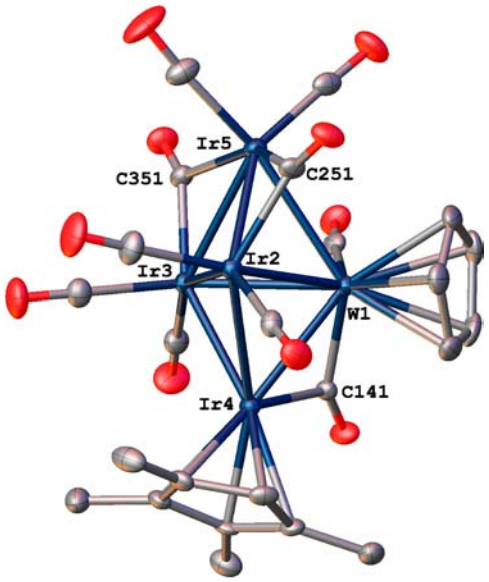

Figure 1. ORTEP plot and atom numbering scheme for **1d**. Displacement ellipsoids are shown at the 30% probability level. Hydrogen atoms have been omitted for clarity.

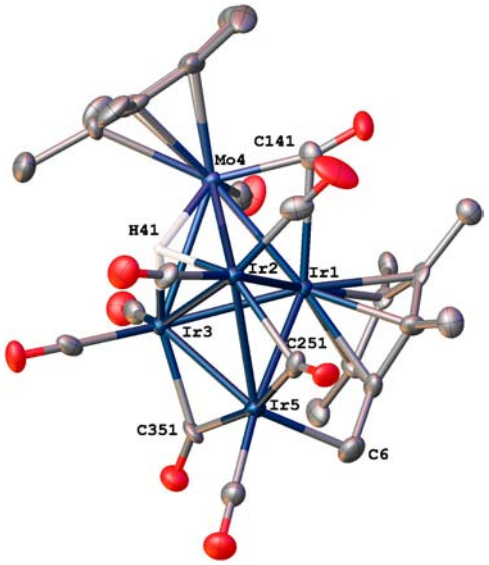

Figure 2. ORTEP plot and atom numbering scheme for **2**. Displacement ellipsoids are shown at the 30% probability level. Hydrogen atoms have been omitted for clarity, with the exception of the hydride ligand (H41), which is shown as a circle of arbitrary radius. Selected bond lengths (Å): Ir1−Ir2 2.7503(7), Ir1−Ir3 2.7632(7), Ir1−Ir5 2.8418(8), Ir1−Mo4 2.6688(12), Ir2−Ir3 2.7961(8), Ir2−Ir5 2.7173(8), Ir2−Mo4 2.9470(13), Ir3−Ir5 2.6960(8), Ir3−Mo4 2.8929(13), Ir1−C141 2.547(17), Mo4−C141 1.959(17), Ir2−C251 2.174(16), Ir5−C251 2.043(18), Ir3−C351 2.111(16), Ir5−C351 2.023(15), Ir5−C6 2.111(17), Ir2−H41 1.85(15), Ir3−H41 1.83(16), Mo4−H41 2.02(15).

The Ir−Ir bonds in clusters **1** fall within a comparatively narrow range [2.7118(4)−2.7716(4) Å]. The Ir−M vectors span a broader range [2.7160(4)−2.8658(7) Å] but are also within literature precedents.[10e] The core bond distances in clusters **3** lie within tighter ranges [Ir−Ir, 2.6991(5)−2.7333(9) Å; Ir−M, 2.7639(7)−2.8475(8) Å; M1−M5, 3.0014(9)−3.0482(9) Å]. Although CO141 symmetrically bridges the

dx.doi.org/10.1021/ic401502f | Inorg. Chem. 2013, 52, 11256−11268

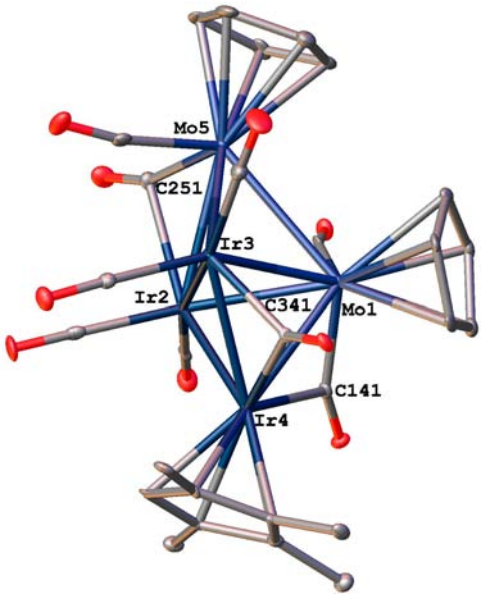

Figure 3. ORTEP plot and atom numbering scheme for **3c**. Displacement ellipsoids are shown at the 30% probability level. Hydrogen atoms have been omitted for clarity.

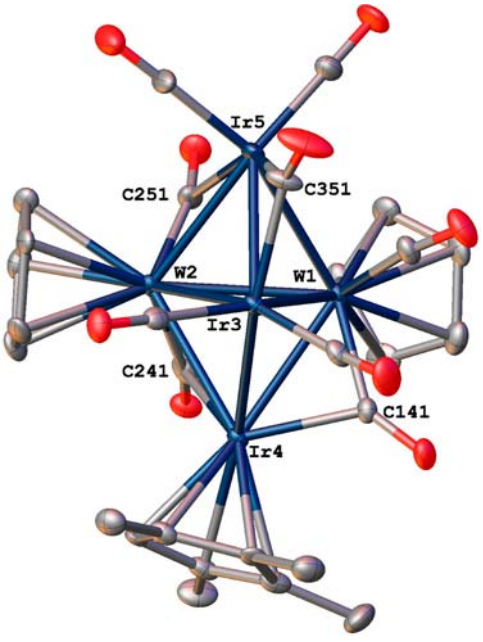

Figure 4. ORTEP plot and atom numbering scheme for **4**. Displacement ellipsoids are shown at the 30% probability level. Hydrogen atoms have been omitted for clarity. Selected bond lengths (Å): W1–W2 2.9237(12), W1–Ir3 2.8235(8), W1–Ir4 2.8013(8), W1–Ir5 2.8337(8), W2–Ir3 2.8369(8), W2–Ir4 2.7822(8), W2–Ir5 2.7910(8), Ir3–Ir4 2.7480(7), Ir3–Ir5 2.7244(8), W1–C141 2.055(12), Ir4–C141 2.066(11), W2–C241 1.981(12), Ir4–C241 2.318(11), W2–C251 1.964(12), Ir5–C251 2.524(13), Ir3–C351 2.085(11), Ir5–C351 2.039(12).

Ir4–M1 vector in clusters **1**, the carbonyl ligands bridging at Ir5 are unsymmetrically disposed toward the other iridium atoms (Ir2, Ir3), with asymmetry parameters[28] for CO251 and CO351 in the range 0.027–0.096, below the nominal semibridging threshold. In contrast, CO341 symmetrically bridges Ir3 and Ir4 in clusters **3**, while bridging CO251 and CO141 are

Table 1. Selected Bond Lengths (Å) for 1a–1d

	1a: M = Mo	**1b**: M = W	**1c**: M = Mo	**1d**: M = W
Ir2–Ir3	2.7339(4)	2.7409(10)	2.7457(6)	2.7525(4)
Ir2–Ir4	2.7576(4)	2.7663(10)	2.7137(7)	2.7213(4)
Ir2–Ir5	2.7552(4)	2.7621(9)	2.7221(6)	2.7268(4)
Ir3–Ir4	2.7118(4)	2.7227(10)	2.7280(6)	2.7362(4)
Ir3–Ir5	2.7349(4)	2.7398(10)	2.7644(6)	2.7716(4)
Ir2–M1	2.8465(7)	2.8422(9)	2.7823(11)	2.7727(4)
Ir3–M1	2.7738(7)	2.7657(9)	2.8474(9)	2.8423(4)
Ir4–M1	2.7329(7)	2.7135(10)	2.7370(10)	2.7160(4)
Ir5–M1	2.8658(7)	2.8461(9)	2.8583(8)	2.8453(4)
Ir2–C251	2.058(8)	2.069(17)	2.039(7)	2.048(7)
Ir5–C251	2.180(7)	2.183(18)	2.146(8)	2.157(7)
Ir3–C351	2.057(9)	2.034(19)	2.023(7)	2.029(7)
Ir5–C351	2.125(8)	2.090(18)	2.215(7)	2.224(7)
Ir4–C141	2.063(7)	2.067(16)	2.068(7)	2.092(7)
M1–C141	2.091(7)	2.067(15)	2.061(7)	2.063(7)

Table 2. Selected Bond Lengths (Å) for 3a–3d

	3a: M = Mo	**3b**: M = W	**3c**: M = Mo	**3d**: M = W
Ir2–Ir3	2.7207(4)	2.7082(8)	2.6991(5)	2.7210(7)
Ir2–Ir4	2.7079(4)	2.7035(7)	2.6993(4)	2.7109(9)
Ir3–Ir4	2.7164(4)	2.7333(9)	2.7184(4)	2.7072(8)
Ir2–M1	2.7899(6)	2.7992(8)	2.7734(7)	2.7695(7)
Ir2–M5	2.7978(7)	2.7923(7)	2.8155(7)	2.7904(9)
Ir3–M1	2.7891(6)	2.7639(7)	2.7827(7)	2.7681(9)
Ir3–M5	2.8258(7)	2.8260(8)	2.8127(7)	2.8198(9)
Ir4–M1	2.8395(6)	2.8388(7)	2.7994(7)	2.8475(8)
M1–M5	3.0482(9)	3.0014(9)	3.0351(9)	3.0165(8)
Ir2–C251	2.382(8)	2.519(12)	2.432(8)	2.499(13)
M5–C251	1.976(8)	1.984(11)	1.967(7)	1.967(12)
Ir3–C341	2.023(8)	2.026(12)	2.017(7)	2.028(11)
Ir4–C341	2.045(7)	1.994(11)	2.043(6)	2.035(11)
Ir4–C141	2.343(7)	2.437(11)	2.284(7)	2.441(12)
M1–C141	1.992(7)	1.978(10)	2.003(8)	2.012(11)

unsymmetrically disposed toward the group 6 metal atoms (asymmetry parameters in the range 0.14–0.27 and therefore formally semibridging). The Ir–Ir and W–Ir bond distances in cluster **4** fall within the aforementioned ranges, and while the W1–W2 vector [2.9237(12) Å] in **4** is shorter than the M1–M5 distances in **3**, it is not anomalously so compared to literature precedents.[10e] As with **3**, CO351 symmetrically bridges an Ir–Ir bond, while bridging carbonyls CO241 and CO251 are displaced toward the group 6 metal (asymmetry parameters 0.17 and 0.28, respectively); in contrast, CO141 symmetrically bridges the W1–Ir4 linkage. Finally, two of the Ir–Ir linkages in **2** are long [Ir2–Ir3, 2.7961(8) Å; Ir1–Ir5, 2.8418(8) Å] and Ir1–Mo4 is short [2.6688(12) Å]; the former are associated with bridging hydrido and η^1:η^5-2,3,4,5-tetramethylcyclopentadienylmethylene ligands, respectively.

Theoretical Studies of 5. The ^{1}H NMR spectrum of **5** contains resonances corresponding to three pentamethylcyclopentadienyl ligands that are in two distinct environments, while the mass spectrum reveals a molecular ion with an EAN-precise electron count for a trigonal-bipyramidal cluster, analogous to the core structures of **1**–**4**. These data are consistent with the Mo(η^5-C_5Me_5) vertices of a trigonal-bipyramidal structure being both apical [Mo(ap)$_2$Ir(eq)] or both equatorial, with the Ir(η^5-C_5Me_5) vertex being apical [Mo(eq)$_2$Ir(ap)] or equatorial [Mo(eq)$_2$Ir(eq)]. DFT calculations were undertaken to

dx.doi.org/10.1021/ic401502f | *Inorg. Chem.* 2013, 52, 11256–11268

discriminate between these possibilities, with the optimized structures being depicted in Figures S7 [Mo(eq)$_2$Ir(ap)], S8 [Mo(eq)$_2$Ir(eq)], and S9 in the SI [Mo(ap)$_2$Ir(eq)]. The calculations reveal that Mo(eq)$_2$Ir(ap) [E_{rel} = 0 kJ mol^{-1}; r[Mo−Ir(η^5-C$_5$Me$_5$)] = 2.89 and 2.92 Å, r(Mo−Mo) = 3.03 Å, r(Mo−Ir$_{CO}$) = 2.84−2.97 Å, Ir$_{CO}$ = non-(η^5-C$_5$Me$_5$)-ligated iridium] is significantly lower in energy than the other possible structures Mo(eq)$_2$Ir(eq) [E_{rel} = +18 kJ mol^{-1}; r[Mo−Ir(η^5-C$_5$Me$_5$)] = 2.92 and 3.06 Å, r(Mo−Mo) = 3.16 Å, r(Mo−Ir$_{CO}$) = 2.83−2.99 Å] and Mo(ap)$_2$Ir(eq) [E_{rel} = +65 kJ mol^{-1}; r[Mo−Ir(η^5-C$_5$Me$_5$)] = 3.02 and 4.56 Å, r(Mo−Ir$_{CO}$) = 2.69−2.92 Å]. Indeed, the structure with apical Mo(η^5-C$_5$Me$_5$) groups optimized to a geometry with a Mo(η^5-C$_5$Me$_5$)−Ir(η^5-C$_5$Me$_5$) bond having cleaved. While this may result from unsustainable steric crowding due to the adjacent pentamethylcyclopentadienyl ligands in this possible core isomer, it is also possible that a different initial placement of carbonyl ligands might not have led to such rupture. The calculations on this species were, in fact, the second optimization attempted for the Mo(ap)$_2$Ir(eq) isomer: the first such attempt (E_{rel} = +107 kJ mol^{-1}) resulted in the loss of one CO ligand but left the trigonal-bipyramidal core more nearly intact [r[Mo−Ir(η^5-C$_5$Me$_5$)] = 3.07 and 3.21 Å; r(Mo−Ir$_{CO}$) = 2.72−2.86 Å]. The calculations clearly suggest that steric crowding has a significant influence on the stability, with the structure with the shortest M(η^5-C$_5$Me$_5$)−M(η^5-C$_5$Me$_5$) distances identified as the lowest-energy isomer, and the set of longest M(η^5-C$_5$Me$_5$)−M(η^5-C$_5$Me$_5$) distances seen in the highest-energy isomer. The most likely structure for **5** is therefore that depicted in Scheme 1.

Electrochemical and Spectroelectrochemical Studies. The electrochemical behavior of the new clusters was assessed by cyclic voltammetry; a representative scan (that of **3a**) is shown in Figure 5, and details from all clusters are collected in Table 3.

All clusters exhibit reduction processes (with respect to the resting state) that are irreversible or partially reversible and for which the reversibility increases upon proceeding to the more iridium-rich clusters **1**. The oxidative behavior of the clusters (with respect to the resting state) is more reversible than the reductive behavior, and increasingly so upon reducing the cluster iridium content, replacing tungsten by molybdenum, and (not surprisingly) increasing the donor strength of the ligands, to the extent that **1a**, **3a**, and **5** exhibit two fully reversible oxidation processes. Where data for reversible processes exist, a small cathodic shift in the oxidation potential is seen upon replacing a tetramethylcyclopentadienyl with a pentamethylcyclopentadienyl coligand and upon replacing the 4d group 6 metal molybdenum with its 5d congener tungsten. Cluster **5**, the only example bearing three strongly electron-donating pentamethylcyclopentadienyl ligands, exhibits a significantly more cathodically shifted oxidation process and is (with **1a** and **3a**) one of only three clusters in the current work to afford two fully reversible oxidation events. A peak height comparison of the oxidative and reductive processes suggests that the former are probably one-electron and the latter are possibly two-electron in nature.

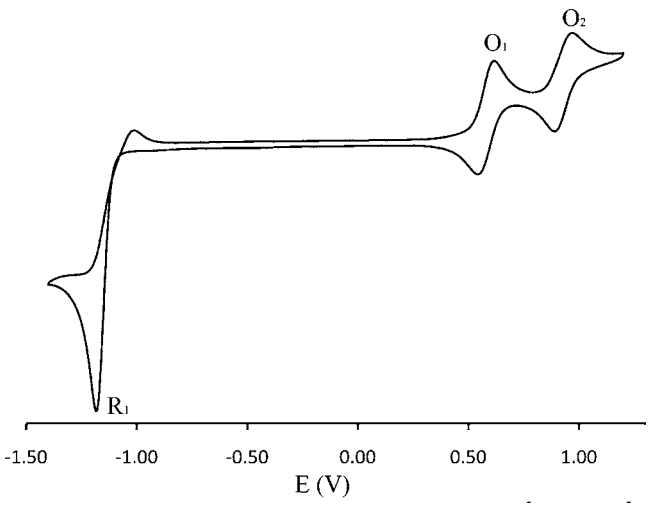

Figure 5. Cyclic voltammogram of **3a** in dichloromethane at room temperature (FcH/FcH$^+$ couple at 0.56 V). Two fully reversible oxidation waves are seen at $E_{1/2}$ = +0.57 and +0.92 V (O_1 and O_2), while an irreversible reduction wave is also seen at $E_{1/2}$ = −1.12 V (R_1).

Table 3. Cyclic Voltammetric Data[a] for 1a−1d, 2, 3a−3d, 4, and 5 and IR Spectroscopic Data for 1a and 3a Following Progressive Oxidation or Reduction

complex	$E_{1/2}$ (i_{pc}/i_{pa}, ΔE) (V)	$E_{1/2}$ (i_{pa}/i_{pc}, ΔE) (V)
1a	0.81 (1, 0.08), 1.06 (1, 0.07)	−0.90 (0.5, 0.08)
1b	0.84[b]	−0.94 (0.7, 0.07)
1c	0.86[b]	−0.89 (0.5, 0.09)
1d	0.84[b]	−0.89 (0.6, 0.09)
2	0.81 (1, 0.08)	−1.32[b]
3a	0.57 (1, 0.08), 0.92 (1, 0.08)	−1.12 (0.5, 0.17)
3b	0.55 (1, 0.09), 0.83 (0.5, 0.05), 1.27[b]	−1.30[b]
3c	0.60,[b] 0.79,[b] 1.26[b]	−1.10[b]
3d	0.58 (1, 0.09), 0.84 (0.6, 0.10), 1.16,[b] 1.40[b]	−1.39[b]
4	0.55 (0.9, 0.09), 0.79 (0.5, 0.04), 0.96,[b] 1.41[b]	−1.27,[b] −1.35[b]
5	0.24 (1, 0.07), 0.80 (1, 0.07)	−1.38[b]
complex	ν(CO) (cm^{-1})	
1a	2052 (s), 2025 (s), 2008 (vs), 1998 (s, sh), 1959 (m), 1942 (w), 1831 (m, br), 1798 (m, br), 1738 (m, br)	
[**1a**]$^+$	2116 (w), 2086 (s), 2050 (s)	
[**1a**]$^{2+}$	2088 (s), 2067 (s), 2052 (vs)	
[**1a**]$^{2-}$	2005 (s), 1962 (vs), 1938 (s), 1898 (m, sh), 1765 (m, br)	
3a	2023 (s), 1996 (vs), 1966 (m), 1950 (w), 1895 (w, br), 1832 (m, br), 1745 (m, br)	
[**3a**]$^+$	2097 (m), 2072 (s), 2060 (m), 2038 (s), 1815 (m, br)	
[**3a**]$^{2+}$	2130 (vw), 2098 (s), 2071 (s), 2039 (s), 2010 (w), 1815 (m, br)	
[**3a**]$^{2-}$	2009 (w), 1985 (w), 1936 (s), 1894 (vs), 1775 (vs, br)	

[a]Conditions: Measurements were carried out at room temperature using platinum disk working, platinum wire auxiliary, and Ag/AgCl reference electrodes, such that the ferrocene/ferrocenium redox couple was located at 0.56 V (i_{pc}/i_{pa} = 1, ΔE_p = 0.09 V). Scan rates were typically 100 mV s^{-1}. Electrochemical solutions contained 0.1 M (NBu$^n_4$)PF$_6$ and ca. 10^{-3} M complex in dried and distilled dichloromethane. [b]E_c or E_a for an irreversible process.

In situ IR and UV−vis spectroscopy using an OTTLE cell was employed to follow the two oxidation steps of **1a** and **3a**, with the results being summarized in Table 3 and displayed in Figures S10−S13 (**1a**) and S14−S17 (**3a**) in the SI. The IR spectrum of the first one-electron oxidation product of **1a**, obtained upon application of a +0.90 V potential, shows a spectral pattern completely different from that of the resting state of **1a**, with this change accompanied by a shift to higher wavenumbers of the terminal carbonyl peaks and the disappearance of the bridging carbonyl bands. The second

dx.doi.org/10.1021/ic401502f | Inorg. Chem. 2013, 52, 11256−11268

oxidation product $\mathbf{1a}^{2+}$, seen when a potential of +1.15 V was applied, is interesting in that the spectral shifts are overall to lower, rather than higher, wavenumbers (unexpected for an oxidative process); this is presumably due to a significant structural rearrangement. The starting cluster is recovered by application of the appropriate potential. A minimal change in the UV−vis spectrum of **1a** occurs with the first oxidation of the cluster, but the second oxidation process results in the formation of a new band at 520 nm, in agreement with postulation of a large structural rearrangement.

The IR spectral changes for the first one-electron oxidation of **3a**, following application of a potential of +0.65 V, show a spectral pattern similar to that of **3a**, but with a shift to higher wavenumbers for the terminal carbonyl peaks and with the appearance of a single broad bridging carbonyl band. Application of a potential of +1.00 V results in formation of the second oxidation product $\mathbf{3a}^{2+}$, which shows minimal spectral change, with the only difference being the appearance of an additional weak absorption at higher wavenumbers and the disappearance of some of the shoulder peaks. Cluster **3a** is regenerated cleanly upon application of the reverse potential. Formation of the oxidation products results in reduction of the intensity of the bands observed in the UV−vis spectra; the resultant spectra are generally featureless.

Theoretical Studies of 1a. DFT and time-dependent DFT (TD-DFT) studies of **1a** were undertaken to rationalize the selectivity for specific core geometry (of the two likely core isomers) and to suggest the nature of the products formed upon reversible oxidation. The reaction of $MoIr_3(\mu\text{-}CO)_3(CO)_8(\eta^5\text{-}C_5H_5)$ with $Ir(CO)_2(\eta^5\text{-}C_5Me_5)$ and formation of a molybdenum tetrairidium cluster is likely to proceed via the addition of the capping $Ir(\eta^5\text{-}C_5Me_5)$ unit at an $MoIr_2$ face (as observed in the present study) or at the less-hindered Ir_3 face. DFT was employed to afford optimized geometries and relative energies for structures based on the X-ray crystallographic study of **1a** and the hypothetical Ir_3 face-capped analogue. The optimized geometries for these structures (in both C_s and C_1 symmetry for the alternate Ir_3 face-capped species) are shown in Figure 6.

Removal of C_s symmetry constraints in the alternate Ir_3 face-capped structure resulted in no significant departure from the optimized geometry obtained with the constraints in place. The starting geometry for the hypothetical structure in Figure 6(ii) was based on the parent cluster $MoIr_3(\mu\text{-}CO)_3(CO)_8(\eta^5\text{-}C_5H_5)$, taking account of the behavior of the $Ir(CO)_2(\eta^5\text{-}C_5Me_5)$ reagent in the experimental reaction, which results in the geometry of Figure 6(i). Adjusting the starting geometry so that the terminal molybdenum-linked carbonyl ligand instead bridges the molybdenum and the relevant equatorial iridium and moving the carbonyl ligand bridging the equatorial and the axial iridium atoms to a terminal position on the axial iridium simply resulted in rearrangement of these ligands to restore essentially the geometry shown in Figure 6(ii) upon optimization. On the basis of the calculations, the experimentally observed structure is essentially equienergetic (~1 kJ mol^{-1} difference) with the alternate Ir_3 face-capped C_s structure. Removal of all symmetry constraints resulted in no further improvement in the stability. Thus, in principle, the Ir_3 face-capped structure is feasible, unless there is a large energy barrier involved in the capping reaction. Computational investigations into the energy barrier for capping either the Ir_3 or $MoIr_2$ face were not undertaken because of the broad range of intermediates that would need to be explored; the overall reaction proceeds with loss of three carbonyl ligands, and there is currently no information available as to how many, if any, of these would be present in a transition state or intermediate.

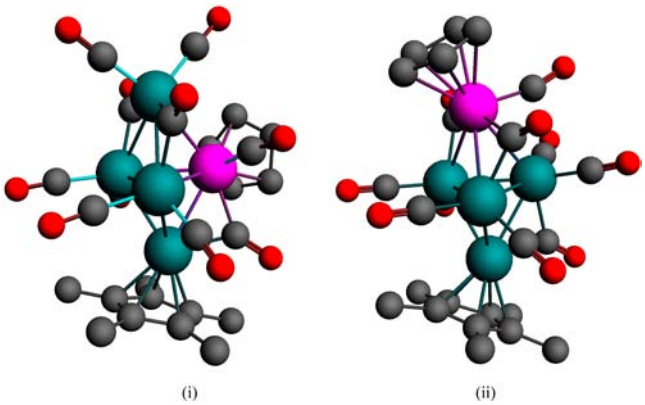

Figure 6. Optimized geometries of **1a** (i) based on the crystal structure and (ii) alternate Ir_3 face-capped structure with C_s symmetry. Color code: fuchsia, Mo; teal, Ir; red, O; gray, C. Hydrogen atoms are omitted for clarity.

We then explored the nature of the oxidation products of **1a**. Optimization of neutral **1a** was performed through spin-restricted, relativistically corrected, vacuum-phase PBE/TZP calculations, using the X-ray crystallographically determined geometry as a starting point. The optimized geometry is consistent with the crystallographically obtained geometry and exhibits carbonyls bridging between Ir2 and Ir5, between Ir3 and Ir5, and between Ir4 and Mo1, as seen in the single-crystal X-ray diffraction structure. Spin-unrestricted calculations on the radical cation and calculations on the dication (singlet state, spin-restricted; triplet state, spin-unrestricted) also consistently identified a structure bridged in this manner (hereafter denoted the "2-5,3-5,4-Mo1" configuration) as a local minimum. The triplet-state dication was found to be 0.45 eV higher in energy than the corresponding singlet-state dication. Solvent-phase (dichloromethane) COSMO calculations on **1a**, $\mathbf{1a}^{+}$, and singlet-state $\mathbf{1a}^{2+}$ similarly determined the 2-5,3-5,4-Mo1 configuration to be a local minimum in each of these charge states. Optimized geometries for the various charge states are summarized in Table 4. It can be seen that optimized bond lengths for the neutral cluster are almost invariably within 0.06 Å of the crystallographic values, for both metal−metal and metal−bridging carbonyl interactions (with only Ir3−Mo1 exaggerated by as much as 0.11 Å). It is also evident that neither inclusion of the solvent effects nor oxidation has a substantial effect on the optimized geometry, confirming the robustness of the cluster geometry at our chosen level of theory.

Because the IR spectra reported here indicate the attenuation of the "bridging CO" feature in the spectrum of oxidized **1a**, we also pursued calculations on all-terminal variants of **1a**, without success. Repeated efforts to isolate all-terminal structures in any charge state, through unconstrained optimizations, instead led to differently bridged isomers of **1a**, as summarized in Table 5. Partial optimizations were finally used to isolate all-terminal structures, with O−C−M bond angles constrained to 178.0°; these geometries, which are not genuine minima (but which we assert to be the lowest-energy structures possessing all-terminal

dx.doi.org/10.1021/ic401502f | Inorg. Chem. 2013, 52, 11256−11268

Table 4. Internuclear Distances Obtained for $1a^{q+}$ (q = 0, 1, 2) from DFT Calculations at the PBE/TZP Level of Theory

r(M−M) (Å)	XRD[a]	q = 0[b]	q = 1[b]	q = 2 (s)[b,c]	q = 2 (t)[d]
Ir2−Ir3	2.7341(4)	2.789/2.782	2.840/2.835	2.912/2.910	2.770
Ir2−Ir4	2.7576(4)	2.739/2.750	2.761/2.774	2.801/2.787	2.764
Ir2−Ir5	2.7552(4)	2.792/2.799	2.770/2.773	2.770/2.768	2.798
Ir2−Mo1	2.8464(7)	2.793/2.800	2.807/2.809	2.872/2.881	2.837
Ir3−Ir4	2.7119(4)	2.773/2.805	2.814/2.830	2.861/2.866	2.805
Ir3−Ir5	2.7348(4)	2.794/2.801	2.758/2.762	2.734/2.738	2.765
Ir3−Mo1	2.7740(7)	2.889/2.888	2.896/2.899	2.916/2.913	2.901
Ir4−Mo1	2.7329(7)	2.775/2.767	2.703/2.691	2.626/2.615	2.662
Ir5−Mo1	2.8656(7)	2.920/2.927	2.968/3.095	2.971/2.961	2.942
Ir2−C251	2.055(8)	2.067/2.060	2.085/2.074	2.112/2.100	2.043
Ir3−C351	2.059(9)	2.060/2.048	2.076/2.062	2.112/2.091	2.017
Ir4−C141	2.061(7)	2.038/2.032	2.048/2.045	2.076/2.078	2.080
Ir5−C251	2.181(8)	2.114/2.112	2.078/2.083	2.038/2.044	2.088
Ir5−C351	2.124(8)	2.175/2.163	2.137/2.132	2.088/2.085	2.246
Mo1−C141	2.090(8)	2.108/2.117	2.113/2.118	2.114/2.111	2.104

[a]Crystal structure geometry. [b]Values shown are respectively from the vacuum-phase and solvent-corrected (dichloromethane) geometry optimizations. [c]Singlet state. [d]Triplet state. Solvent-corrected optimization of this state was not undertaken.

Table 5. Bridging Motifs Found in Isomers of 1a, $1a^+$, and $1a^{2+}$ at the PBE/TZP Level of Theory

charge state	spin state	bridging[a]	E_{rel}(vac)[b,c]	E_{rel}(DCM)[b,d]
0	singlet	none	150.6	164.6
	singlet	**2,5/3,5/4,Mo1**	0.0	0.0
	singlet	2,5/3,5/4,Mo1/4,Mo1	20.7	23.7
1+	doublet	none	81.5	88.3
	doublet	2,4/4,Mo1	−1.2	3.1
	doublet	2,5/3,5/4,Mo1	0.0	0.0
	doublet	2,5/3,4/4,Mo1	4.7	
	doublet	2,5/3,5/4,Mo1/4,Mo1	5.4	8.1
2+	singlet	none	87.4	100.5
	singlet	2,5/3,5/4,Mo1	0.0	0.0
	singlet	2,4/3,Mo1/4,Mo1	−9.6	−5.2
	triplet	none	100.7	
	triplet	3,4	71.3	
	triplet	2,4/3,4,Mo1	33.9	
	triplet	2,5/3,5/4,Mo1	43.0	

[a]Carbonyl-bridged metal centers, where iridium atoms are identified by the numbering shown in the structural study. [b]Relative energy in kJ mol^{-1}, referenced to the [2,5/3,5/4,Mo1] geometry—that is, the structure consistent with the X-ray-diffraction-derived geometry—for that charge state. [c]Vacuum-phase geometry optimization. [d]Solvent-corrected geometry optimization (solvent = dichloromethane). Note that solvent-corrected calculations were not pursued for all geometries. [e]Partial optimization, with O−C−M angles constrained to 178°.

CO ligation), are invariably considerably elevated in energy compared with the bridged structures.

While our calculations do not provide support for the existence of all-terminal clusters in the oxidized forms of **1a**, they do indicate the existence of a substantial variety of bridging motifs. For the neutral cluster, the geometry indicated by the crystal structure is indeed the lowest-energy form that we have isolated, but other bridging motifs appear to be favored (or at least are not significantly disfavored) in the oxidized forms. Increased fluxionality of the carbonyl bridges is a factor that might be expected to influence the observed IR spectra of the oxidized forms.

We have calculated UV−vis spectra for the neutral and cationic forms of **1a** using TD-DFT, at the SAOP/TZP//BP/TZP level of theory. For **1a**, we see a prominent peak at 440 nm, in good agreement with the laboratory result of a peak at ∼410 nm. For $\mathbf{1a}^+$, the calculated spectrum retains this peak, at a slightly larger intensity and mildly blue-shifted to ∼420 nm, with no other significant new features. For $\mathbf{1a}^{2+}$, a similar feature remains visible, again at a slightly greater intensity and mildly blue-shifted to ∼400 nm, with a new spectral feature at ∼500 nm comparing favorably with that seen experimentally at ∼530 nm. The transitions leading to the 440 nm peak in **1a** are dominated by metal-to-ligand charge-transfer (MLCT) character (with the occupied orbitals displaying molybdenum and iridium character and the virtual orbitals displaying a greater degree of character from both the carbonyl and cyclopentadienyl ligands); the 500 nm peak in $\mathbf{1a}^{2+}$ is also dominated by MLCT character, with the key occupied orbitals dominated by iridium and the virtual orbitals displaying cyclopentadienyl-ligand π-bonding character.

DISCUSSION

Our earlier investigations of the reactivity of molybdenum/tungsten triiridium clusters with tricarbonyl(cyclopentadienyl)-metalate anions of the group 6 metals afforded trigonal-bipyramidal M_2Ir_3 clusters in which the group 6 metal atoms are at the apexes [Figure 7(iv)].[12] The present studies extend significantly the range of pentanuclear Mo/W−Ir clusters,

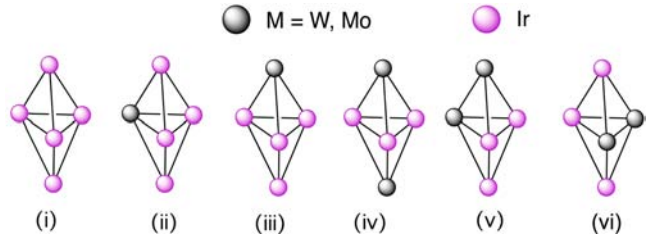

Figure 7. Core geometries of (i) $[P(CH_2Ph)Ph_3]_2[Ir_5(\mu\text{-}H)(\mu\text{-}CO)_2(CO)_{10}]$, $Ir_5(\mu\text{-}CO)_3(\eta^1\text{-}Ph)(CO)_9(PPh_3)$, $Ir_5(\mu\text{-}CO)_4(\mu\text{-}\eta^1,\kappa^1(P)\text{-}C_6H_4\text{-}2\text{-}PPh_2)(CO)_7(PPh_3)$, $Ir_5(\mu\text{-}CO)_4(\eta^1\text{-}Ph)(CO)_7(\eta^2\text{:}\eta^2\text{-}C_8H_{12})$, and $Ir_5(\mu\text{-}CO)_4(\eta^1\text{-}Ph)(CO)_5(\eta^2\text{:}\eta^2\text{-}C_8H_{12})_2$, (ii) **1a**−**1d**, (iii) **2**, (iv) $M_2Ir_3(\mu_3\text{-}H)(\mu\text{-}CO)_2(CO)_9(\eta^5\text{-}C_5H_{5-m}Me_m)(\eta^5\text{-}C_5H_{5-n}Me_n)$ (M = Mo, W; m = 0, 4; n = 4, 5) and $M_2Ir_3(\mu_3\text{-}H)(\mu\text{-}CO)_2(CO)_9(\eta^5\text{-}C_5H_{5-n}Me_n)_2$ (M = Mo, W; n = 4, 5),[12] (v) **3a**−**3d**, and (vi) **4** and **5**.

dx.doi.org/10.1021/ic401502f | Inorg. Chem. 2013, 52, 11256−11268

affording the first examples with the cores depicted in Figures 7(ii) (**1a**−**1d**), 7(iii) (**2**), 7(v) (**3a**−**3d**), and 7(vi) (**4** and **5**) (hereafter referred to as core geometries 7(ii)−7(vi)). The group 6 metal atoms invariably bear cyclopentadienyl ligands in these clusters, but the present studies suggest that this requirement does not preclude the possibility of trimolybdenum/tritungsten diiridium examples on steric grounds, with clusters **3**−**5** demonstrating that the core can accommodate three cyclopentadienyl-ligated metal atoms arranged in either a diapical−equatorial or an apical−diequatorial fashion. Despite this, all extant closo clusters in the group 6 metal−iridium system possess equal numbers of molybdenum/tungsten and iridium, or are iridium-rich, suggestive of a dominant electronic requirement. Together with the previously reported trigonal-bipyramidal pentairidium clusters,[29] the present clusters complete a M_xIr_{5-x} (x = 0−2) core system (Figure 7).

The cluster cores depicted in Figures 7(ii,iii) and 7(iv−vi) afford the possibility of isomers by virtue of differing metal disposition. The formation of the isomers **3d** and **4** (corresponding to differing numbers of bridging carbonyl ligands and a differing metal disposition) is consistent with comparable stability for these examples, while the exclusive formation of **3b** from an analogous reaction differing solely in replacement of the $Ir(CO)_2(\eta^5\text{-}C_5Me_4R)$ (R = H, Me) capping group testifies to the sensitivity of the product outcomes to subtle variations in the reagents. The DFT calculations of **1a** are consistent with this observation, suggesting very little energetic difference between the core isomer possibilities in that case [corresponding to the observed core 7(ii) and the possible core structure 7(iii)]. We have no mechanistic information for the iridium-capping process in the present system, but note that our studies of the capping of $MIr_3(\mu\text{-}CO)_3(CO)_8(\eta^5\text{-}C_5H_{5-n}Me_n)$ (M = Mo, W; n = 0, 4) with the carbonylmetalate anions $[M(CO)_3(\eta^5\text{-}C_5H_{5-n}Me_n)]^-$ (M = Mo, W; n = 4, 5), to afford trigonal-bipyramidal clusters with core geometry 7(iv), are suggestive of a mechanism involving (a) addition, (b) removal of an apical vertex of an intermediate trigonal-bipyramidal cluster to afford a new tetrahedral cluster, and then (c) further addition of a capping unit to afford a new trigonal-bipyramidal cluster.[12] The operative mechanism(s) for capping in these complexes is/are therefore potentially very complex, and speculation is not warranted; in particular, we cannot discard core metal atom fluxionality and, although unlikely, we cannot exclude cyclopentadienyl transfer between iridium atoms, while we have previously noted the inability of DFT to clarify pentanuclear clusters' mechanism(s) of formation.[12]

Cluster **2** exhibits two unique characteristics for this system: its core geometry (Figure 7(iii)) and the C−H activation of a methyl group. There is ample precedent for C−H cleavage of a methyl group of a pentamethylcyclopentadienyl ligand (indeed, C−H cleavage at two methyl groups of a cluster-bound C_5Me_5 ligand has been demonstrated).[30] In the case of **2**, the C−C distances between the ring carbon atoms are all equivalent within experimental error, the C−CH_2 distance [C1−C6, 1.45(2) Å] is not significantly shorter than the ring C−CH_3 distances [1.49(2)−1.51(2) Å], and Ir5−C1 is too long for a significant bonding interaction [2.696(17) Å]; an η^1:η^5-tetramethycyclopentadienylmethylene description (rather than a η^2:η^4-fulvene interaction) therefore seems more appropriate.

Cyclic voltammetry studies revealed cathodic shifts in the oxidation potential upon replacing molybdenum by tungsten and upon increasing alkylation of the cyclopentadienyl ligands that mimic those observed at the precursor tetrahedral clusters.[9q] In the present series of trigonal-bipyramidal clusters, the oxidation processes are increasingly reversible upon reducing the iridium content of the clusters, replacing tungsten by molybdenum, and increasing alkylation of the cyclopentadienyl ligands, mirroring observations with their tetrahedral precursors.[9q] A comparison of the electrochemical data of the current series of clusters with that of their precursors[9q] revealed an increase in the reversibility and a cathodic shift of the first oxidation process upon introduction of the capping group. In situ IR and UV−vis−near-IR (NIR) spectroelectrochemical studies of the reversible oxidation processes in **1a** and **3a** suggested progression to an all-terminal CO geometry concomitant with the first oxidation and a significant structural change upon the second oxidation step. Similarly, IR spectroelectrochemical studies of $W_2Ir_2(CO)_{10}(\eta\text{-}C_5H_4Me)_2$ (the methylcyclopentadienyl analogue of a precursor tetrahedral cluster in the present system) revealed an analogous progressive disappearance of bridging CO bands on a first oxidation step.[9q]

DFT and TD-DFT have been used previously to rationalize structural and spectroscopic data for molybdenum/tungsten−iridium clusters[9q,s,u,12] as well as to predict their first hyperpolarizabilities.[31] The present studies have exploited DFT in conjunction with spectroscopic data to suggest a likely structure for **5** (with the probable alternatives being considerably higher in energy). DFT studies have also revealed that the crystallographically confirmed Mo-equatorial core geometry of **1a** is essentially isoenergetic with a possible Mo-apical isomer, the latter a core geometry observed with the C−H activated product **2**. Calculations on charged states of **1a** identified several bridging CO structures, in contrast to the spectroscopic data that suggest an all-terminal CO disposition, reiterating the caution that one must apply in tackling medium-nuclearity clusters comprised of 4d and 5d metal atoms with DFT. The UV−vis−NIR spectroelectrochemical data obtained upon progressive oxidation to afford $\mathbf{1a}^{2+}$ revealed the appearance of a broad low-energy band centered at ca. 520 nm for the doubly oxidized species that TD-DFT calculations suggest has significant Ir → cyclopentadienyl character. Oxidation of the smaller $W_2Ir_2(CO)_{10}(\eta^5\text{-}C_5H_4Me)_2$ revealed the appearance of a similar low-energy band in the UV−vis−NIR spectrum, assigned by TD-DFT as primarily σ(W−W) → σ*(W−W) in nature.[9q] The cluster core metal atoms are clearly crucial for the low-energy bands observed in the spectra of both the tetra- and pentanuclear clusters.

The present studies have demonstrated the utility of $Ir(CO)_2(\eta^5\text{-}L')$ (L′ = C_5Me_5, C_5Me_4H) as capping reagents in effecting a core-nuclearity increase in this mixed-metal cluster system. While considerable success has been achieved with cluster expansion using $M(L)_2Cp$ reagents (M = Co, Rh, Ir; L = CO, alkene; Cp = C_5H_5, C_9H_7) in previous studies,[9c,32] these earlier reactions condense the group 9 metal reagent with an unsaturated species, either those incorporating an alkylidene ligand or those possessing multiple M−M bonding (preexisting or generated in situ). Indeed, $M(CO)_2(\eta^5\text{-}C_5H_5)$ (M = Rh, Ir) was identified as an undesirable byproduct that impeded cluster formation in some reactions employing $M(\eta^2\text{-}C_2H_4)_2(\eta^5\text{-}C_5H_5)$.[32i,j] We have previously shown that replacing cyclopentadienyl with tetra/pentamethylcyclopentadienyl in carbonylmetalate reagents is essential to achieving redox condensation with the tetrahedral clusters $MIr_3(\mu\text{-}CO)_3(CO)_8(\eta^5\text{-}C_5H_{5-n}Me_n)$ (M = Mo, W; n = 0, 4);[12] in the present case,

dx.doi.org/10.1021/ic401502f | Inorg. Chem. 2013, 52, 11256−11268

significant alkylation of the iridium capping reagents similarly enhances their nucleophilicity, sufficient to ensure condensation and cluster nuclearity increases.

CONCLUSION

Mixed-metal cluster chemistry has focused strongly on lower-nuclearity species (M_n, n = 3, 4) primarily because of the lack of efficient routes to higher-nuclearity examples. The present studies have now afforded access to a systematically varied suite of trigonal-bipyramidal clusters M_nIr_{5-n} (n = 0−2) exhibiting all possible core metal dispositions. The cyclic voltammetry studies herein have revealed that the redox potentials of these clusters are a function of the cluster composition (nature of group 6 metal, group 6−group 9 metal ratio, and degree of alkylation of cyclopentadienyl ligand), and so the electron richness of the cluster can be controlled by composition modification. The lowest-lying transitions in such clusters involve significant metal atom character, so linear optical, nonlinear-optical, and optical limiting properties are potentially strongly influenced by core metal variation; the present series affords the possibility of testing this idea in a systematic fashion.

Mixed-metal clusters have long been touted as potential precursors to heterobimetallic catalysts, in which the specific metal dispositions and local environments can be controlled because the ligand sheath can be removed under mild conditions (indeed, tetrahedral examples MIr_3 and M_2Ir_2 with this same mixed-metal combination show differing behavior toward butane hydrogenolysis); the M_nIr_{5-n} clusters, with their varying core metal dispositions, will permit studies exploring these possibilities, with the greater diversity inherent in pentanuclear cluster precursors. The present report also highlights the utility of $Ir(CO)_2(\eta^5\text{-}L')$ (L' = C_5Me_5, C_5Me_4H) as a capping reagent to effect a core-nuclearity increase in cluster chemistry and the necessity of using highly alkylated cyclopentadienyl ligands to ensure sufficiently nucleophility in the capping reagent.

ASSOCIATED CONTENT

Supporting Information

X-ray crystallographic data in CIF format, crystal data for **1a**−**1d**, **2**, **3a**−**3d** and **4**, ORTEP plots of **1a**−**1c**, **3a**, **3b**, and **3d**, DFT-optimized geometries of possible isomers of **5**, and IR and UV−vis spectral data during progressive oxidation of **1a** and **3a**. This material is available free of charge via the Internet at http://pubs.acs.org. Crystallographic data for the structural analyses have also been deposited with the Cambridge Crystallographic Data Centre, under CCDC 912502 (**3b**), 912503 (**4**), 912504 (**3d**), 912505 (**1c**), 912506 (**3c**), 912507 (**1a**), 912508 (**3a**), 912509 (**1d**), 912510 (**2**), and 912511 (**1b**). Copies of this information may be obtained, free of charge, from the Director, CCDC, 12 Union Road, Cambridge CB2 1E2, U.K. (fax +44-1223-336033, e-mail deposit@ccdc.cam.ac.uk, or www http://www.ccdc.cam.ac.uk).

Related Articles

Mixed-Metal Cluster Chemistry. Part 33. Part 32: Randles, M. D.; Gupta, V.; Simpson, P. V.; Moxey, G. J.; Criddle, A. L.; Stranger, R.; Cifuentes, M. P.; Humphrey, M. G. *Polyhedron* **2013**, *52*, 957.

AUTHOR INFORMATION

Corresponding Author

*E-mail: Mark.Humphrey@anu.edu.au. Tel: +61 2 6125 2927. Fax: +61 2 6125 0750.

Notes

The authors declare no competing financial interest.

ACKNOWLEDGMENTS

We thank the Australian Research Council (ARC) for financial support. M.D.R. was the recipient of an Australian Postgraduate Award, and J.F. was the recipient of a China Scholarship Council ANU Postgraduate Scholarship. S.R.B. thanks the ARC for a Future Fellowship, M.P.C. thanks the ARC for an Australian Research Fellowship, and M.G.H. thanks the ARC for an Australian Professorial Fellowship.

REFERENCES

(1) Braunstein, P.; Oro, L. A.; Raithby, P. R. *Metal Clusters in Chemistry*; Wiley-VCH: Weinheim, Germany, 1999.

(2) de Jongh, L. J. *Physics and Chemistry of Metal Cluster Compounds*; Kluwer: Dordrecht, The Netherlands, 1994.

(3) Adams, R. D.; Cotton, F. A. *Catalysis by Di- and Polynuclear Metal Cluster Complexes*; Wiley-VCH: New York, 1998.

(4) Zhang, C.; Song, Y. L.; Wang, X. *Coord. Chem. Rev.* **2007**, *251*, 111.

(5) Waterman, S. M.; Lucas, N. T.; Humphrey, M. G. *Adv. Organomet. Chem.* **2000**, *46*, 47.

(6) (a) Ciani, G.; Moret, M.; Sironi, A.; Antognazza, P.; Beringhelli, T.; D'Alfonso, G.; Della Pergola, R.; Minoja, A. *J. Chem. Soc., Chem. Commun.* **1991**, 1255. (b) Hao, L.; Vittal, J. J.; Xiao, J.; Puddephatt, R. J. *J. Am. Chem. Soc.* **1995**, *117*, 8035.

(7) (a) Bergamo, M.; Beringhelli, T.; D'Alfonso, G.; Ciani, G.; Moret, M.; Sironi, A. *Organometallics* **1996**, *15*, 1637. (b) Beringhelli, T.; Ceriotti, A.; Ciani, G.; D'Alfonso, G.; Garlaschelli, L.; Della Pergola, R.; Moret, M.; Sironi, A. *J. Chem. Soc., Dalton Trans.* **1993**, 199. (c) Henly, T. J.; Shapley, J. R.; Rheingold, A. L.; Gelbb, S. J. *Organometallics* **1988**, *7*, 441. (d) Henly, T. J.; Wilson, S. R.; Shapley, J. R. *Inorg. Chem.* **1988**, *27*, 2551.

(8) (a) Stone, F. G. A. *Angew. Chem., Int. Ed. Engl.* **1984**, *23*, 89. (b) Davies, S. J.; Howard, J. A. K.; Musgrove, R. J.; Stone, F. G. A. *Angew. Chem., Int. Ed. Engl.* **1989**, *28*, 624. (c) Davies, S. J.; Howard, J. A. K.; Musgrove, R. J.; Stone, F. G. A. *J. Chem. Soc., Dalton Trans.* **1989**, 2269. (d) Elliot, G. P.; Howard, J. A. K.; Mise, T.; Moore, I.; Nunn, C. M.; Stone, F. G. A. *J. Chem. Soc., Dalton Trans.* **1986**, 2091. (e) Davies, S. J.; Stone, F. G. A. *J. Chem. Soc., Dalton Trans.* **1989**, 785. (f) Carr, N.; Mullica, D. F.; Sappenfield, E. L.; Stone, F. G. A.; Went, M. J. *Organometallics* **1993**, *12*, 4350. (g) Davies, S. J.; Elliot, G. P.; Howard, J. A. K.; Nunn, C. M.; Stone, F. G. A. *J. Chem. Soc., Dalton Trans.* **1987**, 2177. (h) Elliot, G. P.; Howard, J. A. K.; Nunn, C. M.; Stone, F. G. A. *J. Chem. Soc., Chem. Commun.* **1986**, 431. (i) Elliot, G. P.; Howard, J. A. K.; Mise, T.; Nunn, C. M.; Stone, F. G. A. *Angew. Chem., Int. Ed. Engl.* **1986**, *25*, 190. (j) Elliot, G. P.; Howard, J. A. K.; Mise, T.; Nunn, C. M.; Stone, F. G. A. *J. Chem. Soc., Dalton Trans.* **1987**, 2189.

(9) (a) Comstock, M. C.; Shapley, J. R. *Coord. Chem. Rev.* **1995**, *143*, 501. (b) Schacht, H.-T.; Vahrenkamp, H. *Chem. Ber.* **1989**, *122*, 2239. (c) Neumann, H.-P.; Ziegler, M. L. *J. Organomet. Chem.* **1989**, *377*, 255. (d) Ziegler, M. L.; Neumann, H.-P. *Chem. Ber.* **1989**, *122*, 25. (e) Richter, F.; Müller, M.; Gärtner, N.; Vahrenkamp, H. *Chem. Ber.* **1984**, *117*, 2438. (f) Pasynskii, A. A.; Eremenko, I. L.; Orazsakhatov, B.; Kalinnikov, V. T.; Aleksandrov, G. G.; Struchkov, Y. T. *J. Organomet. Chem.* **1981**, *214*, 367. (g) Eremenko, I. L.; Pasynskii, A. A.; Katugin, A. S.; Orazsakhatov, B.; Shirokii, V. L.; Shklover, V. E.; Struchkov, Y. T. *J. Organomet. Chem.* **1988**, *345*, 177. (h) Churchill, M. R.; Biondi, L. V. *J. Organomet. Chem.* **1989**, *366*, 265. (i) Shapley, J. R.; McAteer, C. H.; Churchill, M. R.; Biondi, L. V. *Organometallics* **1984**, *3*, 1595. (j) Churchill, M. R.; Biondi, L. V.; Shapley, J. R.; McAteer, C.

H. *J. Organomet. Chem.* **1985**, *280*, C63. (k) Churchill, M. R.; Biondi, L. V. *J. Organomet. Chem.* **1988**, *353*, 73. (l) Churchill, M. R.; Li, Y.-J.; Shapley, J. R.; Foose, D. S.; Uchiyama, W. S. *J. Organomet. Chem.* **1986**, *312*, 121. (m) Lee, J.; Humphrey, M. G.; Hockless, D. C. R.; Skelton, B. W.; White, A. H. *Organometallics* **1993**, *12*, 3468. (n) Lucas, N. T.; Humphrey, M. G.; Hockless, D. C. R. *J. Organomet. Chem.* **1997**, *535*, 175. (o) Waterman, S. M.; Humphrey, M. G. *Organometallics* **1999**, *18*, 3116. (p) Waterman, S. M.; Lee, J.; Humphrey, M. G.; Ball, G. E.; Hockless, D. C. R. *Organometallics* **1999**, *18*, 2440. (q) Lucas, N. T.; Blitz, J. P.; Petrie, S.; Stranger, R.; Humphrey, M. G.; Heath, G. A.; Otieno-Alego, V. *J. Am. Chem. Soc.* **2002**, *124*, 5139. (r) Lucas, N. T.; Notaras, E. G. A.; Cifuentes, M. P.; Humphrey, M. G. *Organometallics* **2003**, *22*, 284. (s) Lucas, N. T.; Notaras, E. G. A.; Petrie, S.; Stranger, R.; Humphrey, M. G. *Organometallics* **2003**, *22*, 708. (t) Notaras, E. G. A.; Lucas, N. T.; Humphrey, M. G.; Willis, A. C.; Rae, A. D. *Organometallics* **2003**, *22*, 3659. (u) Usher, A. J.; Dalton, G. T.; Lucas, N. T.; Waterman, S. M.; Petrie, S.; Stranger, R.; Humphrey, M. G.; Willis, A. C. *J. Organomet. Chem.* **2004**, *689*, 50. (v) Randles, M. D.; Lucas, N. T.; Cifuentes, M. P.; Humphrey, M. G.; Smith, M. K.; Willis, A. C.; Samoc, M. *Macromolecules* **2007**, *40*, 7807. (w) Randles, M. D.; Gupta, V.; Simpson, P. V.; Moxey, G. J.; Criddle, A. L.; Stranger, R.; Cifuentes, M. P.; Humphrey, M. G. *Polyhedron* **2013**, *52*, 957.

(10) Core nuclearity M_n, n = 5: (a) Davies, S. J.; Howard, J. A. K.; Pilotti, M. U.; Stone, F. G. A. *J. Chem. Soc., Chem. Commun.* **1989**, 190. (b) Davies, S. J.; Howard, J. A. K.; Pilotti, M. U.; Stone, F. G. A. *J. Chem. Soc., Dalton Trans.* **1989**, 1855. (c) Tunik, S. P.; Shipil, P. N.; Vlasov, A. V.; Denisov, V. R.; Nikols'kii, A. B.; Dolgushin, F. M.; Yanovsky, A. I.; Struchkov, Y. T. *J. Organomet. Chem.* **1996**, *515*, 11. (d) Waterman, S. M.; Humphrey, M. G.; Tolhurst, V.-A.; Bruce, M. I.; Low, P. J.; Hockless, D. C. R. *Organometallics* **1998**, *11*, 5789. (e) Dalton, G. T.; Viau, L.; Waterman, S. M.; Humphrey, M. G.; Bruce, M. I.; Low, P. J.; Roberts, R. L.; Willis, A. C.; Koutsantonis, G. A.; Skelton, B. W.; White, A. H. *Inorg. Chem.* **2005**, *44*, 3261. (f) Randles, M. D.; Dewhurst, R. D.; Cifuentes, M. P.; Humphrey, M. G. *Organometallics* **2012**, *31*, 2582. n = 6: (g) Notaras, E. G. A.; Lucas, N. T.; Humphrey, M. G. *J. Organomet. Chem.* **2001**, *631*, 139. (h) Ref 10e. n = 7: (i) Waterman, S. M.; Humphrey, M. G.; Hockless, D. C. R. *Organometallics* **1996**, *15*, 1745.

(11) Mo/W–Ir butane hydrogenolysis studies: (a) Shapley, J. R.; Humphrey, M. G.; McAteer, C. H. In *Selectivity in Catalysis*; Davis, M. E., Suib, S. L., Eds.; American Chemical Society: Washington, DC, 1993; p 127. (b) Shapley, J. R.; McAteer, C. H.; Churchill, M. R.; Biondi, L. V. *Organometallics* **1984**, *3*, 1595. (c) Shapley, J. R.; Hardwick, S. J.; Foose, D. S.; Stucky, G. D. *J. Am. Chem. Soc.* **1981**, *103*, 7383. (d) Shapley, J. R.; Uchiyama, W. S.; Scott, R. A. *J. Phys. Chem.* **1990**, *94*, 1190. Mo–Co desulfurization studies: (e) Riaz, U.; Curnow, O.; Curtis, M. D. *J. Am. Chem. Soc.* **1991**, *113*, 1416. (f) Mansour, M. A.; Curtis, M. D.; Kampf, J. W. *Organometallics* **1995**, *14*, 5460. (g) Mansour, M. A.; Curtis, M. D.; Kampf, J. W. *Organometallics* **1997**, *16*, 3363. (h) Riaz, U.; Curnow, O. J.; Curtis, M. D. *J. Am. Chem. Soc.* **1994**, *116*, 4357. (i) Curtis, M. D. *J. Cluster Sci.* **1996**, *7*, 247. (j) Curtis, M. D.; Druker, S. H. *J. Am. Chem. Soc.* **1997**, *119*, 1027. (k) Curtis, M. D.; Penner-Hahn, J. E.; Schwank, J.; Baralt, O.; McCabe, D. J.; Thompson, L.; Waldo, G. *Polyhedron* **1988**, *7*, 2411. For reviews of mixed-metal cluster catalysis, see: (l) Braunstein, P., Rosé, J., Eds. *Heterometallic Clusters in Catalysis*; Elsevier: Amsterdam, The Netherlands, 1989; Vol. 3. (m) Braunstein, P.; Rosé, J. In *Comprehensive Organometallic Chemistry II*; Abel, E. W., Stone, F. G. A., Wilkinson, G., Eds.; Pergamon: Oxford, U.K., 1994; Vol. *10*, Chapter 7.

(12) Usher, A. J.; Lucas, N. T.; Dalton, G. T.; Randles, M. D.; Viau, L.; Humphrey, M. G.; Petrie, S.; Stranger, R.; Willis, A. C.; Rae, A. D. *Inorg. Chem.* **2006**, *45*, 10859.

(13) Ball, R. G.; Graham, W. A. G.; Heinekey, D. M.; Hoyano, J. K.; McMaster, A. D.; Mattson, B. M.; Michel, S. T. *Inorg. Chem.* **1990**, *29*, 2023.

(14) Mahr, A.; Nürnberg, O.; Werner, H. *Z. Anorg. Allg. Chem.* **2003**, *629*, 91.

(15) Otwinowski, Z.; Minor, W. *Methods Enzymol.* **1997**, *276*, 307.

(16) Blessing, R. H. *Acta Crystallogr., Sect. A: Fundam. Crystallogr.* **1995**, *51*, 33.

(17) *Apex II*, version 2.1; Bruker AXS Ltd.: Madison, WI, 2007.

(18) Betteridge, P. W.; Carruthers, J. R.; Cooper, R. I.; Prout, K.; Watkin, D. J. *J. Appl. Crystallogr.* **2003**, *36*, 1487.

(19) Sheldrick, G. M. *Acta Crystallogr., Sect. A: Fundam. Crystallogr.* **2008**, *64*, 112.

(20) Dolomanov, O. V.; Bourhis, L. J.; Gildea, R. J.; Howard, J. A. K.; Puschmann, H. *J. Appl. Crystallogr.* **2009**, *42*, 339.

(21) van der Sluis, P.; Spek, A. L. *Acta Crystallogr., Sect. A: Fundam. Crystallogr.* **1990**, *46*, 194.

(22) (a) *Amsterdam Density Functional, Scientific Computing and Modelling, Theoretical Chemistry*; Vrije Universiteit: Amsterdam, The Netherlands (http://www.scm.com). (b) Fonseca Guerra, C.; Snijders, J. G.; te Velde, G.; Baerends, E. J. *Theor. Chem. Acc.* **1998**, *99*, 391. (c) te Velde, G.; Bickelhaupt, F. M.; van Gisbergen, S. J. A.; Fonseca Guerra, C.; Baerends, E. J.; Snijders, J. G.; Ziegler, T. *J. Comput. Chem.* **2001**, *22*, 931.

(23) Parr, R.; Yang, W. *Density Functional Theory of Atoms and Molecules*; Oxford University Press: New York, 1989.

(24) Vosko, S.; Wilk, L.; Nusair, M. *Can. J. Chem.* **1980**, *58*, 1200.

(25) Petrie, S.; Stranger, R. *Inorg. Chem.* **2004**, *43*, 2597.

(26) Becke, A. *J. Chem. Phys.* **1993**, *98*, 5648.

(27) van Lenthe, E.; Ehlers, A. E.; Baerends, E. J. *J. Chem. Phys.* **1999**, *110*, 8943.

(28) (a) Curtis, M. D.; Butler, W. M. *J. Organomet. Chem.* **1978**, *155*, 131. (b) Klingler, R. J.; Butler, W. M.; Curtis, M. D. *J. Am. Chem. Soc.* **1978**, *100*, 5034.

(29) (a) $[P(CH_2Ph)Ph_3]_2[Ir_5(\mu\text{-}H)(\mu\text{-}CO)_2(CO)_{10}]$: Pergola, R. D.; Garlaschelli, L.; Manassero, M.; Sansoni, M.; Strumolo, D. *J. Cluster Sci.* **2001**, *12*, 23. (b) $Ir_5(\mu\text{-}CO)_3(\eta^1\text{-}Ph)(CO)_9(PPh_3)$ and $Ir_5(\mu\text{-}CO)_4(\mu\text{-}\eta^1,\kappa^1(P)\text{-}C_6H_4\text{-}2\text{-}PPh_2)(CO)_7(PPh_3)$: Adams, R. D.; Chen, M. *Organometallics* **2011**, *30*, 5867. (c) $Ir_5(\mu\text{-}CO)_4(\eta^1\text{-}Ph)(CO)_7(\eta^2\text{:}\eta^2\text{-}C_8H_{12})$ and $Ir_5(\mu\text{-}CO)_4(\eta^1\text{-}Ph)(CO)_5(\eta^2\text{:}\eta^2\text{-}C_8H_{12})_2$: Adams, R. D.; Chen, M. *Organometallics* **2012**, *31*, 445.

(30) Selected examples of C–H cleavage of a methyl group of a C_5Me_5 ligand. (a) C–H cleavage at two methyl groups of a hafnium-bound ligand: Beweries, T.; Burlakov, V. V.; Peitz, S.; Bach, M. A.; Arndt, P.; Baumann, W.; Spannenberg, A.; Rosenthal, U. *Organometallics* **2007**, *26*, 6827. (b) C–H cleavage at one methyl group of a zirconium-bound ligand: Burlakov, V. V.; Arndt, P.; Baumann, W.; Spannenberg, A.; Rosenthal, U. *Organometallics* **2006**, *25*, 519. (c) C–H cleavage at two methyl groups of a yttrium (or lutetium)-bound ligand: Shima, T.; Hou, Z. *Organometallics* **2009**, *28*, 2244. (d) C–H cleavage at one methyl group of a cluster-bound ligand: Clegg, W.; Feeder, N.; Nahar, S.; Raithby, P. R.; Shields, G. P.; Teat, S. J. *New J. Chem.* **1998**, 1111. (e) C–H cleavage at two methyl groups of a cluster-bound ligand: Wang, W.; Davis, H. B.; Einstein, F. W. B.; Pomeroy, R. K. *Organometallics* **1994**, *13*, 5113.

(31) (a) Li, F.; Liu, C.; Liu, C.; Wu, K. *Mol. Phys.* **2007**, *105*, 2251. (b) Li, F.-J.; Sa, R.-J.; Wu, K.-C. *Chin. J. Struct. Chem.* **2009**, *28*, 99.

(32) (a) Etches, S. J.; Hart, I. J.; Stone, F. G. A. *J. Chem. Soc., Dalton Trans.* **1989**, 2281. (b) Abad, J. A.; Delgado, E.; Garcia, M. E.; Grosse-Ophoff, M. J.; Hart, I. J.; Jeffery, J. C.; Simmons, M. S.; Stone, F. G. A. *J. Chem. Soc., Dalton Trans.* **1987**, 41. (c) Green, M.; Howard, J. A. K.; James, A. P.; Jelfs, A. M. de M.; Nunn, C. M.; Stone, F. G. A. *J. Chem. Soc., Chem. Commun.* **1984**, 1623. (d) Green, M.; Howard, J. A. K.; James, A. P.; Nunn, C. M.; Stone, F. G. A. *J. Chem. Soc., Dalton Trans.* **1986**, 187. (e) Green, M.; Jeffery, J. C.; Porter, S. J.; Razay, H.; Stone, F. G. A. *J. Chem. Soc., Dalton Trans.* **1982**, 2475. (f) Bermúdez, M. D.; Brown, F. P. E.; Stone, F. G. A. *J. Chem. Soc., Dalton Trans.* **1988**, 1139. (g) Doyle, R. A.; Angelici, R. J.; Stone, F. G. A. *J. Organomet. Chem.* **1989**, *378*, 81. (h) Hill, A. F.; Marken, F.; Nasir, B. A.; Stone, F. G. A. *J. Organomet. Chem.* **1989**, *363*, 311. (i) Walther, B.; Scheer, M.; Böttcher, H.-C.; Trunschke, A.; Ewald, H.; Gutschick, D.; Miessner, H.; Skupin, M.; Vorbeck, G. *Inorg. Chim. Acta* **1989**, *156*, 285. (j) Winter, G.; Schulz, B.; Trunschke, A.; Miessner, H.; Böttcher, H.-C.; Walther, B. *Inorg. Chim. Acta* **1991**, *184*, 27. (k) Chisholm, M. H.;

Johnston, V. J.; Eisenstein, O.; Streib, W. E. *Angew. Chem., Int. Ed. Engl.* **1992**, *31*, 896. (l) Bantel, H.; Powell, A. K.; Vahrenkamp, H. *Chem. Ber.* **1990**, *123*, 677.